J. Fluid Mech. (2006), *vol.* 549, *pp.* 25–59.
doi:10.1017/S0022112005007482 Printed in the United Kingdom

Laterally converging duct flows. Part 3. Mean turbulence structure in the viscous layer

By DONALD M. McELIGOT[1] AND HELMUT ECKELMANN[2]

[1]Idaho National Laboratory (INL), Idaho Falls, ID 83415-3885 USA and University of Arizona, Tucson, AZ 85721 USA

[2]Institut für Nichtlineare Dynamik, Universität Göttingen, D37073 Göttingen, Deutschland and Max-Planck-Institut für Dynamik und Selbstorganisation (formerly Max-Planck-Institut für Strömungsforschung), Bunsenstr. 10, D37073 Göttingen, Germany

(Received 18 June 2003 and in revised form 1 July 2005)

In order to provide fundamental bases for incorporating the effects of favourable streamwise pressure gradients into models for internal turbulent flows and turbulent boundary layers, time series measurements with a cross-wire probe and a wall shear stress sensor were obtained simultaneously in an oil channel both for fully developed and laterally converging flows. Data were concentrated in the viscous layer and at the centreplane for slight to highly favourable pressure gradients. (Here the viscous layer is defined as the region where viscous effects are significant, but not necessarily dominant; it includes the 'laminar' and buffer sublayers in the terminology of some investigators). Results presented include comparisons of the profiles of the mean statistics, plus correlations and spectra, of streamwise and wall-normal components, their product and the wall shear stress. The key new data are the measurements of the fluctuating normal component and related statistics in the viscous layer for highly favourable pressure gradients. For the outer half of the viscous layer its root-mean-square fluctuations decrease as the pressure gradient is increased, consistent with heretofore unconfirmed predictions from direct numerical simulations. Based on examination of the probability density distributions, one may conclude that an effect of a strong pressure gradient is to reduce transport of momentum in the outer part of the viscous layer.

1. Introduction

Laterally converging flow is one version of a group of flows which lead to favourable streamwise pressure gradients and, consequently, may modify characteristics of a turbulent flow. 'Strong' favourable pressure gradients have been found to reduce viscous drag by altering the structure of the turbulent velocity fluctuations. In fact, with a favourable non-dimensional pressure gradient K_p of the order of -0.03 an apparent 'laminarization' of a turbulent boundary layer can occur (Narasimha & Sreenivasan 1979). ($K_p = (\nu/\rho u_\tau^3)\,\mathrm{d}p/\mathrm{d}x$ where ν, ρ, u_τ, p and x denote kinematic viscosity, fluid density, friction velocity, static pressure and streamwise coordinate, respectively.) Others include sink flows (Spalart 1986; Jones, Marusic & Perry 2001), nozzle flows (Launder 1964), flows around the leading edges of wings and turbine blades and vanes (Mayle 1991), strongly heated internal gas flows (Shehata & McEligot 1998) and fully developed duct and tube flows (Kim, Moin & Moser 1987; Durst, Jovanovic & Sender 1995). In the last case, it is known, but apparently not well, that a low-Reynolds-number turbulent flow may involve a strong favourable pressure gradient even though the flow is fully developed and therefore not accelerating spatially.

In the idealized case, a laterally converging flow is two-dimensional in circular coordinates, i.e. in the streamwise direction, the flow is radially inward; this situation is exemplified by flow between parallel disks with an exit at the centre of one. This paper is the third in a sequence delving successively deeper into the structure of laterally converging turbulent flows. The first considered the mean flow in terms of the streamwise pressure distribution and wall shear stress as well as applying a simple mixing-length model for their numerical prediction (Murphy, Chambers & McEligot 1983, hereinafter referred to as MCM). The second by Chambers, Murphy & McEligot (1983, hereinafter referred to as CMM) measured the temporal wall shear stress and analysed it via the VITA technique of Blackwelder & Kaplan (1976).

The present work concentrates on the mean turbulence structure in the viscous layer because it is typically the region where the largest gradients occur and the turbulence production is largest. Following Bradshaw (1975), we are here defining the viscous layer as the region where viscous effects are significant, but not necessarily dominant, typically to y^+ about 30 in a classical zero-pressure gradient case (it includes the 'laminar' and buffer sublayers in some terminology). The quantity y is the normal distance from the wall and the superscript $^+$ here and later represents normalization by wall units, ν and friction velocity $u_\tau (= (\tau_w/\rho)^{1/2}$ with τ_w symbolizing the mean wall shear stress). The dominant uncertainties in momentum, energy and mass transfer resistances occur in this layer. Liepmann years ago and Ichimiya (1995) suggested that this region limits the turbulence fluctuations from the free stream and others note that a solid wall damps primarily the turbulent fluctuations in the normal direction, causing strong anisotropy, as it is approached (e.g. Hanjalic, Jakirlic & Hadzic 1997). With a significant favourable pressure gradient, the popular constant shear layer idealization is weakened, e.g. for a well-developed flow, the total shear stress τ is given by $(\tau\{y\}/\tau_w) \approx 1 + K_p y^+$, so for $K_p = -0.02$, $\tau\{y\}$ decreases 60 % within the viscous layer (the subscript w here and later denotes evaluation at the wall). To examine the viscous layer, the present study employed the oil channel designed by Reichardt at the Max Planck Institut für Strömungsforschung (now Max-Planck-Institut für Dynamik und Selbstorganisation) to give excellent spatial resolution in this region.

Previous studies of flows with favourable streamwise pressure gradients have been summarized by Narasimha & Sreenivasan (1979), Spalart (1986) and MCM/CMM. Considerable effort has been expended to identify criteria for modification and laminarization and scaling to correlate the behaviour of dependent variables. An effect of a favourable pressure gradient is to 'thicken' the viscous layer, in some senses; bursting rates are reduced (Kline *et al.* 1967; CMM). The consequent upward shift in the logarithmic region as the Reynolds number is lowered was identified by McEligot, Ormand & Perkins (1966) via the mean velocity measurements of Senecal (1952). Until recently, experimental constraints have normally made measurement of v – and therefore of uv to deduce the Reynolds shear stress – impractical. Throughout the remainder of this paper, the streamwise velocity is represented as $\tilde{u} = U + u$, where the tilde denotes an instantaneous quantity and upper and lower case letters symbolize the corresponding mean value and the fluctuation about it, respectively; the normal velocity $\tilde{v}$ is treated in a similar fashion. In recent years, scholarly work has mostly been devoted to attempts to simulate flows with pressure gradients numerically, particularly with a variety of turbulence models (e.g. Hanjalic, Hadzic & Jakirlic (1999)). Experimental measurements for strong favourable pressure gradients are still sparse, particularly for the viscous layer (McEligot & Eckelmann 2003, table 1).

Based on definitions, continuity and momentum equations and empirical relations, we can form approximate relations between some of the non-dimensional parameters suggested as governing the flows. Streamwise acceleration is often represented by an acceleration parameter (Kline *et al.* 1967) defined as

$$K_v = \left(\nu/U_\infty^2\right) \mathrm{d}U_\infty/\mathrm{d}x.$$

The subscript infinity indicates evaluation in the free stream. For a boundary-layer flow, we can show $K_v = -(c_f/2)^{3/2} K_p$ where c_f is the skin friction coefficient, defined as $(2\tau_w/(\rho U_\infty^2))$. For fully developed flow in a duct, K_v is zero by definition and the pressure-gradient parameter may be estimated as

$$K_p = \left(\nu/\rho u_\tau^3\right) \mathrm{d}p/\mathrm{d}x = \sim -20.1\, Re_{D,h}^{-(7/8)}$$

by employing a Blasius correlation (Patel 1965). The Reynolds number $Re_{D,h}$ here is based on the bulk or mixed mean velocity and on the hydraulic diameter D_h calculated as four times the cross-sectional area divided by the 'wetted' perimeter of the duct. Consequently, some authors may have interpreted 'pressure-gradient effects' as 'low-Reynolds-number effects' and others may not have realized that their fully developed internal flow could have entailed significant streamwise pressure gradients. The distance y_c to the centreplane, centreline or other thickness measure can be represented as

$$y_c^+ = (y_c u_\tau/\nu) = (y_c/D_h)\, Re_{D,h} (c_f/2)^{1/2} = \sim 0.20 (y_c/D_h)\, Re_{D,h}^{7/8}.$$

This quantity is also denoted as $Re_\tau (= y_c u_\tau/\nu)$ by some investigators (e.g. Kim *et al.* 1987).

When can the viscous layer be expected to be affected by a streamwise pressure gradient? The governing momentum equation may be written

$$U^+(\partial U^+/\partial x^+) + V^+(\partial U^+/\partial y^+) = -K_p + (\partial \tau^+/\partial y^+).$$

Near the wall, the solution for the total shear stress variation can be approximated (Julien, Kays & Moffat 1969; Finnicum & Hanratty 1988) as

$$\tau^+\{y^+\} = (\tau\{y^+\}/\tau_w) = 1 + K_p y^+ [1 - (c_f/(2y^+)) \int_0^{y^+} (U^+)^2\, \mathrm{d}y^+].$$

(The braces $\{\}$ are used to indicate that τ^+ is considered to be a function of y^+.) For a fully developed flow in a duct or tube, the convective terms become zero by definition and this solution reduces to

$$\tau^+\{y^+\} = (\tau\{y^+\}/\tau_w) = 1 + K_p y^+,$$

as mentioned earlier. For the effect of a pressure gradient to be negligible in the viscous layer, we could establish a criterion that τ^+ still be greater than 0.95 or such at its edge (say $y^+ \approx 30$). This constraint translates to requirements such as $-K_p < 0.0017$, $Re_{D,h} > 46\,000$ for channels and y_c^+ or $Re_\tau > 600$. In this sense, a 'low-Reynolds-number' duct flow is inherently affected by a streamwise pressure gradient.

The success of Bradshaw's overlapping internal boundary-layer approach for ducts (Bradshaw, Dean & McEligot 1973) implies that the turbulence in half of a duct is affected by the lower-velocity eddies transported from the other half. If sufficiently close, the consequent effect on the turbulence could affect the region near the viscous layer and, in turn, the viscous layer itself. Thus, for the viscous-layer behaviour to be similar in various geometries and flows, we need (i) the viscous layer to be small

relative to geometric scales, and (ii) to have the same distribution of $\partial\tau^+\{y^+\}/\partial y^+$ through the viscous layer. If we estimate that a distance of 10 y_v^+ would be adequate to avoid interaction with other walls or free stream, it would lead to the requirement that s^+, δ^+, r_w^+ or $W^+/2$ (as appropriate) be greater than about 300. (The quantity y_v^+ is an estimate of the viscous-layer thickness, δ^+ is the boundary-layer thickness, r_w^+ is the pipe radius and W^+ is the the side length of a square tube, all in wall coordinates.) Then we would expect reasonable agreement between viscous-layer results for a tube and a channel at the same K_p and same y_c^+ provided that y_c^+ is more than about 300. For the channel, this requirement corresponds to $-K_p < \sim 0.0033$ and $Re_{D,h} > \sim 21\,000$.

From the momentum equation, we see the distribution of $\partial\tau^+\{y^+\}/\partial y^+$ will be a function of K_p alone provided the convective terms are zero or negligible. Fully developed flows in tubes, channels and parallel-plate ducts inherently satisfy this requirement. In the present viscous-layer study, the effect of the convective terms is found to increase as y^+ and/or $|K_p|$ increase. One sees the magnitude of the convective term in τ^+ will be less than $K_p y^+ c_f (U^+)^2/2$; taking half this value as an order-of-magnitude approximation, we can estimate that the effect of the convective terms will be 5 % or less, provided that $-K_p$ is about 0.006 or less. This value corresponds to $y_c^+ \approx 170$ for parallel plates and 330 for circular tubes. So, for lower $|K_p|$ and higher y_c^+, results for accelerating flows should agree with those from the fully developed results in the viscous layer at the same K_p. As $|K_p|$ increases to higher values, the results should diverge as the convective terms become more important; the trends with K_p should be the same, but magnitudes would differ at the same K_p. Above this level, a given value of K_p for an accelerating flow would correspond to a lower value for the fully developed flow, since the convective terms counter the pressure gradient in the expression for τ^+.

Some investigators have suggested conditions for 'low-Reynolds-number' effects to become negligible, usually based on observation of the approximate logarithmic region of a turbulent wall flow. Since the resulting level of a logarithmic curve fit through data is a consequence of integration through the viscous layer, these conditions imply criteria for affecting the viscous layer. Moser, Kim & Mansour (1999, hereinafter referred to as MKM99) indicated that their direct numerical simulations at $Re_\tau = 590$ appear free of the most obvious low-Reynolds-number effects; this value corresponds to $-K_p \approx 0.0017$ (as suggested above). For their pipe flow, Durst *et al.* (1996) mention that their velocity profile at $Re_D = 13\,600$ ($K_p \approx -0.0049$) agrees with an asymptotic logarithmic 'law' written as $u^+ = 2.5 \ln y^+ + 5$. Here and later we employ the traditional definition $u^+ = (U/u_\tau)$ without confusion since fluctuations are not mentioned directly in wall coordinates. Examining the channel flow measurements of Durst *et al.* (1998) and comparing them to the logarithmic correlation, we can estimate that for this geometry a value of $-K_p < 0.0068$ gives slight effects (less than 5 % difference), $-K_p > 0.011$ or so gives strong effects (more than 10 %) and in between these values, effects are expected to be moderate. (These values of $-K_p$ are above our approximate estimate for independence from geometry effects.)

1.1. *Previous studies*

While the details of many accelerating flows have been extensively studied (Murphy 1979; Narasimha & Sreenivasan 1979), few appear to have used lateral convergence between parallel plates to examine turbulent flows with strong positive streamwise pressure gradients (MCM; CMM; Singh, Vyas & Powle 1999). In the idealized problem, the velocity is uniform at an entry at a large distance. The flow develops and

may approach a fully established profile. Near the exit of the convergence, acceleration dominates the flow in the centre of the duct, causing a flattening of the profile. The profile takes the appearance of an external boundary-layer flow, with a large central core flanked on both sides with thin boundary layers. The boundary layers become successively thinner as acceleration continues. Depending on the entrance length and flow rate, the regime may be laminar or turbulent, or an initially turbulent flow may approach a laminar flow owing to the stabilizing effects of acceleration or a favourable pressure gradient, i.e. so-called 'laminarization' may occur.

Analyses predicting the effects of streamwise pressure gradients on turbulent boundary layers are now available from the work of MKM99 and Abe, Kawamura & Matsuo (2001) for slight effects plus Spalart (1986) and Finnicum & Hanratty (1988). Spalart conducted direct numerical simulations of sink-flow boundary layers with acceleration parameters K_v between 1.5×10^{-6} and 3.0×10^{-6}. He solved the three-dimensional time-dependent Navier–Stokes equations using a spectral method. Predicted effects of the favourable pressure gradients were to extend and displace the logarithmic layer and to alter the energy balance of turbulence near the edge of the boundary layers. Relaminarization was predicted for $K_v = 3.0 \times 10^{-6}$ (approximately $-K_p = 0.025$). Reasonable agreement was found with the spatial spectra deduced by Jones & Launder (1972) from their temporal spectra data at $K_v = 1.5 \times 10^{-6}$ except that Spalart's computed spectra did not collapse versus y. In general, his results suggested that the logarithmic behaviour of the mean velocity is more universal than the linear behaviour of a mixing-length model. Spalart compared his predictions of r.m.s. velocity fluctuations for $K_v = 1.5 \times 10^{-6}$ and 2.5×10^{-6} and found the peak value of $(u')^+$ to be about 2.35 in both cases. (The prime indicates that the root-mean-square value of the fluctuation is being presented.) The peak values of $(v')^+$ and $(w')^+$ decreased about 20 % and 25 %, respectively, as K_v (and $-K_p$) was increased.

Finnicum & Hanratty applied the two-and-a-half dimensional computational model of Nikolaides (1984) with bursting periods and streak spacing taken to vary as the ratio between the wall shear stress and the mean shear stress at the assumed edge of the viscous layer (their y_o^+). Empirical results were used for skin friction coefficients. Phase relations at y_o^+ were assumed to be unchanged by the pressure gradient. For a range $K_v = 0$, 2.0×10^{-6} ('moderate') and 2.8×10^{-6} ('close to relaminarization') they predicted mean statistics of u and v and appropriate terms for kinetic energy balances. Good agreement was seen with the direct numerical simulations of Spalart (1986).

While duct flows can involve significant streamwise pressure gradients, most of the direct numerical simulations have concentrated on conditions near Eckelmann's lower-Reynolds-number measurements (1974) at Re_s about 5400 or slightly more (e.g. Kim *et al.* (1987), hereinafter referred to as KMM) so $-K_p$ was about 0.0068 or less. The definition of Re_s is based on the centreplane velocity U_c and the plate spacing s. MKM99 extended the approach of KMM for fully developed channel flow at low Reynolds numbers to higher flow rates. As the Reynolds number was reduced ($-K_p$ increased), they found a slight reduction in the profile of the r.m.s. streamwise velocity component and larger reductions for the normal and spanwise components.

The direct numerical simulations generally predict that, as a favourable streamwise pressure gradient is increased, there is no significant change in the streamwise component, but that the normal and spanwise fluctuations would decrease observably.

Quantitative turbulence structure measurements with significant pressure gradients are limited. In the past, they have often been limited to data with a single sensor,

particularly in the viscous layer, owing to probe size concerns using air or water as the fluid. Jones & Launder (1972) found that the peak Reynolds stress due to turbulence became a progressively smaller fraction of the wall shear stress as $K_u = (\nu/U_\infty^2)\,\mathrm{d}U_\infty/\mathrm{d}x$ increased. In a study of large-scale motion, Blackwelder & Kovasznay (1972) found that, when K_u exceeded 'critical' values, the viscous sublayer thickness increased, the skin-friction coefficient at the wall decreased and large departures from the turbulent logarithmic law of the wall occurred; to some extent, these aspects can be predicted using advanced (and some simple) turbulence models (McEligot & Bankston 1969; Rodi 1980).

For laterally converging laminar flow between parallel plates, Murphy, Coxon & McEligot (1978) extended the numerical approach of Bankston & McEligot (1970), as well as developing a similarity solution. MCM then applied the numerical program to the conditions of an experiment they conducted with turbulent and apparently laminarizing air flow converging between two plates separated by 1.3 cm (1/2 in). With streamwise acceleration, the flow was continuously developing through the entry region and downstream. Measurements were restricted to streamwise pressure distributions and wall shear stress, since the spacing necessary and wall shear layers were too small to introduce probes into the flow to determine the velocity distribution. By comparison between data and predictions, they found substantial effects to occur with convergence angles as small as 4° and showed that the results could be explained by a thickening of the viscous layer.

In the same apparatus, CMM applied conditional sampling, by the VITA technique of Blackwelder & Kaplan (1976), to the instantaneous measurements of wall shear stress. They found the typical burst pattern, or conditionally averaged time history of the wall shear stress, resembled the time history of the streamwise velocity component measured by Blackwelder & Kaplan at $y^+ = 15$. Families of conditionally averaged time histories were selected at approximately equal Reynolds numbers and varying acceleration parameters to compare with the results for fully developed flows.

For this flow problem, the results of MCM and CMM can be summarized as follows: (i) for $K_v > 4 \times 10^{-6}$, laminar predictions are adequate for pressure distributions and friction factors; (ii) for $K_v < 10^{-7}$, the simple van Driest (1956) model provides reasonable predictions; (iii) the temporal wall shear signal was consistent with these observations; and (iv) as K_v increased, the non-dimensional bursting frequency decreased, but the conditionally averaged signal remained approximately constant until large K_v.

Sano & Asako (1993) and Sano & Shirakashi (1994) obtained measurements in a duct with one wall alternately converging and diverging in a streamwise-periodic fashion, giving a continuously varying, oscillating pressure gradient. For the two configurations studied, maximum values of $|K_p|$ of about 0.02 and 0.03 were reached. Wall coordinates were estimated by fitting the linear layer, $u^+ = y^+$, as far from the wall as possible. (For a zero-pressure-gradient flow, this technique would underestimate the wall shear stress.) Sano & Asako concentrated on presenting the variations of friction factor, $U\{y\}$, $u'\{y\}$ and heat transfer parameters. They concluded that significant changes appeared only in the diverging section, i.e. unfavourable pressure gradient. Sano & Shirakashi employed a cross-wire probe as well as a single wire and presented statistical measures of the observed behaviour, such as spectra, correlations and probability density distributions. For the streamwise component, some results were presented at estimated locations $y^+ \approx 10$, 15 and 20 in the viscous layer, but only for $y^+ \approx 100$ for the normal component v. They concluded that the wavenumber region between the maximum and minimum eddy scales becomes

narrower in the accelerating region so that the eddy scale was decreasing (in physical coordinates rather than being non-dimensionalized with wall coordinates).

The present work supplements several experiments on turbulent boundary layers with streamwise pressure gradients. Ichimiya (1995) measured distributions of streamwise mean velocity and turbulent fluctuations in a turbulent boundary, which later experienced transition towards a laminar one and then relaxed as the flow converged from a square duct to a narrower rectangular duct of the same width. The resulting streamwise pressure gradient and acceleration parameters increased to peaks and then decreased to constant and negligible values. The intermittency distribution was also measured. Instantaneous time series and other statistical quantities were obtained at $y^+ \approx 30$. Escudier *et al.* (1998) obtained data for streamwise mean velocity and fluctuations and intermittency in a comparable experiment. In both experiments, acceleration parameters above 4×10^{-6} were achieved and measurements were taken with single hot wires so measurements of v (and uv) are not available in the viscous layer.

Castillo & George (2001) considered the outer flow at high Reynolds numbers to identify equilibrium boundary layers and found supporting data in earlier experiments; their region of interest was well beyond the viscous layer as their treatment required $y^+ > 100$ and $\delta^+ > 500$. Jones *et al.* (2001) measured turbulent boundary layers in sink flows at high Reynolds numbers. With acceleration parameters K_v from 2.7×10^{-7} to 5.4×10^{-7}, they realized favourable pressure gradients ($-K_p$) between 0.0033 and 0.0054, approximately the same range as the DNS of MKM99 for fully developed duct flow. While they were able to measure u' to y^+ as low as about twelve with a single wire, the thin boundary layers and shear effects across the cross-wire probe limited data for v' (and $\overline{uv}$ for the Reynolds shear stress $= -\rho\overline{uv}$ where the overbar denotes the time mean value of the product of the fluctuations u and v) to y^+ greater than 40 (I. Marusic, personal communication 2005). Spalart & Watmuff (1993) conducted an experiment with a varying streamwise pressure gradient to study effects of unfavourable pressure gradients. However, their first measurement station provided profiles for $K_v \approx 1.25 \times 10^{-6}$ and $Re_\theta > \sim 600$, giving $-K_p \approx 0.008$ which is slightly higher than those of Jones *et al.* The sensor lengths of their small cross-wire probe were about $7.5 < l_s^+ < 13$ or about five times larger than the present probe (in wall units). They noted difficulties near the wall and found measured values of v' (and w' where w represents the spanwise velocity component) to be considerably less than their DNS predictions in that region. Warnack & Fernholz (1998) and Fernholz & Warnack (1998) measured turbulence distributions in axisymmetric turbulent boundary layers with the acceleration varying in the streamwise direction to give laminarizing and laminarescent conditions; peak values of $-K_p$ ranged from 0.014 to 0.033, approximately. For their profiles with significant streamwise pressure gradients, the actual measurements with a cross-wire probe for $\tilde{v}$ and $\overline{uv}$ and their statistics were outside the viscous layer.

Durst *et al.* (1995) used a laser Doppler velocimeter with refractive-index-matching techniques to determine distributions of u', v' and w' in fully developed flow in a circular tube (here w represents the circumferential velocity component). With a minimum Reynolds number of 7440, their values of $-K_p$ were about 0.008 or less. By going to lower Reynolds numbers, Durst *et al.* (1996, 1998) reached values of K_p of about -0.014 (tube) and -0.012 (channel), but only streamwise quantities were reported.

Extensive detailed measurements (u, v, w, etc.) in the viscous layers of fully developed channel flows have been reported by Eckelmann and coworkers (Eckelmann

1974; Brodkey, Wallace & Eckelmann 1974; Kreplin & Eckelmann, 1979*a–c*). These experiments were at $U_c s/\nu = 5400$ ($Re_{D,h} \approx 9300$) or higher, so $-K_p$ was about 0.0068 or less.

In summary, there is evidence that the turbulence structure is modified by streamwise pressure gradients and there is a need to determine which features remain relatively invariant in the viscous layer and to quantify the variation of the others in order to provide the turbulence structure information required in models accounting for their effects. Spalart's DNS predictions of a reduction of $(v')^+$ for high-pressure gradients do not appear to have been verified yet by experiments. Measurements of v and uv are required. Until recently such measurements were usually not practical because of spatial constraints. Now with laser-Doppler anemometry (Ching, Djenidi & Antonia 1995; Fontaine & Deutsch 1995) in conjunction with refractive-index-matching techniques (Thiele & Eckelmann 1994; Durst *et al.* 1995; Becker *et al.* 2002) and low velocities, we can measure v (hence uv) with good spatial resolution and adequate precision to values of y^+ less than unity. However, the flows identified using these methods have only been applied for measurements of v (and uv) in slight streamwise pressure gradients. The present study extends the experiments of Eckelmann and colleagues to a laterally converging configuration to give time series data for u, v, uv and τ_w for slight to strong favourable pressure gradients.

2. Experiment

In accordance with the needs indicated, the objectives of the present study are to determine which features of the turbulence structure remain relatively invariant in the viscous layer, to quantify the variation of the others with moderate to strong streamwise pressure gradients and to confirm or refute the DNS predictions of reductions in $(v')^+$ with increasingly favourable pressure gradients. The experiments performed used the oil channel at the Max Planck Institut für Strömungsforschung. This facility was designed originally by Reichardt to give high spatial and temporal resolution in the viscous layer and has since been developed by Eckelmann (1974) and his colleagues (Wallace, Eckelmann & Brodkey 1972; Wallace, Brodkey & Eckelmann 1977; Blackwelder & Eckelmann 1978; Kreplin & Eckelmann 1979*a*, *c*; etc.)

The oil channel and procedures employed in its use have been described in detail by Eckelmann (1974). In this section, we will concentrate on the differences in apparatus and techniques applied for the present study; only a brief overview will be given for the aspects which are in common with the earlier work. Further details are provided in a technical report by McEligot & Eckelmann (2003).

The channel is 22 cm wide and 1 m deep with a length of 8 m (figure 1 of Eckelmann 1974). In contrast to the 1.3 cm spacing in the experiment of MCM, the plates forming this oil channel have much larger separation, so area blockage by the probes is negligible. Also, at $Re_{D,h} \approx 11\,000$ a distance of 1 cm corresponds to $y^+ = 17$, permitting high spatial resolution. The use of oil as working fluid and low velocities leads to higher temporal resolution of fluctuating components than in the common fluids, air and water. Velocity measurements are made with commercial hot-film probes which are calibrated via a time-of-flight technique moving the support cart along the channel.

For measurements with laterally converging flow, the channel floor was modified to a convergence angle of 2° (figure 1) giving a potential intermediate range of acceleration parameters $1 \times 10^{-6} < K_v < 3 \times 10^{-6}$ as desired to examine conditions where the turbulence structure was expected to be modified. Data acquisition programs were

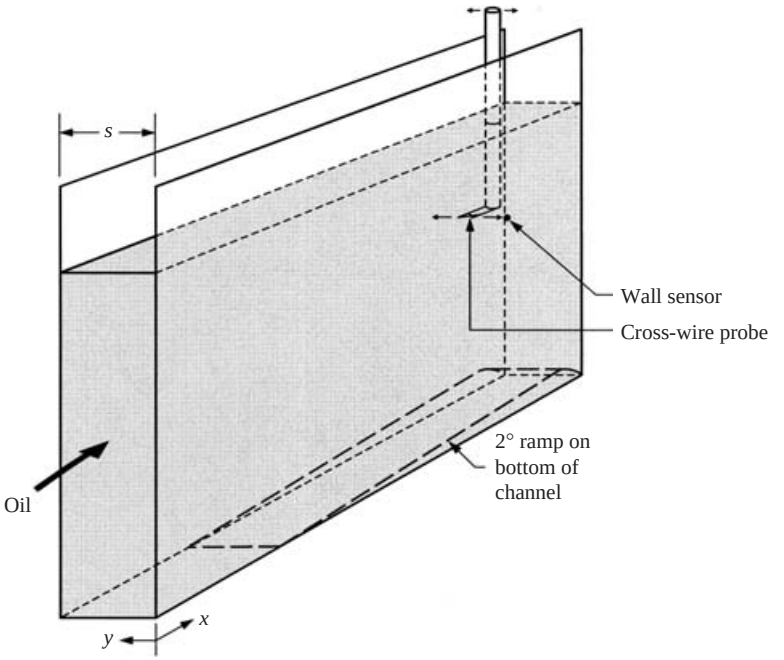

FIGURE 1. Schematic diagram of experimental configuration (not to scale).

modified for digital application of the hot-film calibration as a function of the oil temperature at low overheat ratios. Experimental studies of flow-induced vibrations were conducted in order to design probe supports for measurements deep in the channel near the lower surface.

One original concept of this oil channel, without convergence, was to approximate an infinitely long parallel-plate channel by using the same dimensions for the return channel as for the test section and by employing a specially designed turning pump and turning vanes (see the plan view in figure 1 of Eckelmann 1974). For flow development, the oil passes along a return channel approximately thirty spacings long before passing through a series of curved vanes in a 180° bend, which forms the entrance to the test channel. With a typical depth of 80 cm, the aspect ratio is about 3.6 for the open channel; with the free surface approximating a zero shear surface, this configuration is comparable to a closed channel with an aspect ratio of 7. In the test channel, with the ramp installed as shown schematically in figure 1, the entrance region of $\Delta x/s \approx 15$ provides for further flow development ahead of the section of length $\Delta x/s \approx 17$ converging to the minimum cross-section ('throat'). The main measurements in the converging section are taken at $x/s \approx 31$ (or about one spacing ahead of the throat), where a wall sensor is also mounted.

For direct comparison, measurements approximating fully developed conditions ($K_V \approx 0$) were obtained by removing the ramp from the bottom of the channel. Otherwise, locations remained the same. In an open-channel flow with a horizontal floor and constant spacing of the walls, there is an inherent streamwise acceleration as the fluid depth decreases while overcoming the wall friction; for the cases investigated here, the equivalent K_v was less than 10^{-8}.

Instantaneous velocity measurements were obtained with hot-film cross-wire probes, a TSI model 1241 with bent prongs and a Disa type 55R61; a photograph of the

former is shown by Johnson & Eckelmann (their figure 4, 1983). The non-dimensional sizes of these probes were: cylinder diameter $\sim 0.07 < d^+ < \sim 0.12$, sensor length $\sim 1.3 < l_s^+ < \sim 2.2$ and sensor spacing $\sim 1.3 < s_s^+ < 2.2$, varying with experimental conditions. No correction for sensor spacing was applied for the data; typical spacing was of the order of one to two Kolomogorov lengths. The sensors were operated via a Disa 55M01 anemometer system.

For both velocity probes, the sensors were calibrated by the time-of-flight technique of Eckelmann (1974). The calibration technique has been described by Eckelmann and the use of the calibration carriage on the channel is demonstrated in his figure 1. The estimated uncertainty during calibration was based on the uncertainties in distance and timing; it varied from about 0.03 % at low velocity to 0.1 % at the highest velocity. Reproducibility of the imposed velocity varied from 0.15 % to 0.23 %. The calibration data for each sensor were fit with a fourth-order polynomial of velocity as a function of measured voltage, as developed by Randolph (1983). Typical agreement between the polynomial and the data was of the order of 0.2 % and less.

Time series data were acquired via a DEC PDP-15 system from four hot-film sensors simultaneously: a cross-wire probe for $\tilde{u}\{t, y\}$ and $\tilde{v}\{t, y\}$, a wall element for $\tau_w\{t\}$ and a single fixed upstream sensor to serve as a reference (the symbol t denotes time). Measurements were taken in the viscous layer ($y^+ \approx 5$, 7, 10, 15, 25) and at the centreplane for $K_v = 1.6 \times 10^{-6}$ and $K_v = 2.4 \times 10^{-6}$ for the cases with streamwise acceleration. Maximum significant turbulence frequencies were less than 5 Hz and bursting frequencies were estimated to be of the order of 0.1 Hz or less. Some additional measurements of mean turbulence quantities for fully developed flow in the same channel are available at approximately the same Reynolds numbers for comparison (Eckelmann 1974; Randolph 1983, 1987).

Klewicki & Falco (1990) reviewed earlier data to estimate the averaging times necessary to deduce turbulence statistics accurately from time-series measurements with thermal sensors. For channel flows, the most demanding requirement found was a non-dimensional duration ($2TU_c/s$) greater than 5000 required by Eckelmann *et al.* (1977) for ensemble averages in the Ölkanal of the present experiment. From their own boundary-layer studies, Klewicki & Falco concluded that – to ensure accuracy of 3 % – averaging times (TU_∞/δ) of 1000 were required for mean and r.m.s. results and 4000 for skewness factors. In the present experiment, durations ($2TU_c/s$) of 5545 to 7390 were employed.

The uncertainty in the mean-square value of a fluctuating quantity, such as $(u')^2$ (or $(v')^2$), can be estimated to be

$$\sigma_{(u')^2} \approx [(u')^2]^{1/2}/(N/2)^{1/2}$$

where σ_u is the random uncertainty in u and N is the number of independent realizations (Metzger 2002). This approximation can be rearranged to provide the estimated experimental uncertainty in u' as $\sigma_u' \approx (\sigma_u/2)/(N/2)^{1/2}$ and correspondingly for v'. The number of realizations can be estimated from the duration of the measurements divided by a characteristic time deduced from a characteristic length (possibly an 'eddy' size in a turbulent boundary layer) and a characteristic velocity. For a channel, the characteristic length might be considered to be its spacing, depth or length with the last being the most conservative (i.e. fewest realizations). In earlier studies with the same channel, Kreplin found that – in order to achieve a reproducible mean value of the velocity within 1 % – measuring times of 20 to 30 min were necessary at $Re_s \approx 7700$ and 15 to 40 min at $Re_s \approx 4700$ (Kreplin 1973, 1976; Eckelmann personal communication 2005). Kreplin's observations are consistent with

the selection of channel length as the characteristic dimension. For the present estimates of uncertainties in u' and v', we employed the centreline velocity and the conservative choice of channel length. Consequently, for our 200 000 samples over 4000 s, the number of independent realizations was estimated to be about 70 to 90, depending on the experimental run.

For the cross-wire probe, the overheat ratio is set at about 5 % (rather than the more common 1 % or 2 %) in order to reduce sensitivity to gradual temperature variations. Despite control of the room temperature, these precautions are necessary to reduce the uncertainties in the velocities to below 1 %. Development of the temperature correction factor is summarized by McEligot & Eckelmann (2003, Appendix A).

The theodolite technique of Eckelmann (1974) was employed to set the reference location of the crossing of the sensors of the cross-wire probe to within about ± 0.1 mm. For $y < 30$ mm, a dial indicator with an estimated reading uncertainty of ± 0.002 mm was used to determine transverse locations relative to this reference. Beyond that distance a vernier rule was employed; it could be read to ± 0.1 mm.

With oil, the streamwise pressure gradient corresponding to a significant value of K_p is minuscule. Thus, it was difficult to obtain an accurate measurement of $\mathrm{d}p/\mathrm{d}x$ for determining τ_w (see § 3) and K_p. Several methods were considered and/or attempted (McEligot & Eckelmann 2003, Appendix A). Ultimately, a 'hook gauge technique' was applied (using a point gauge) (Marks 1916, p. 287). Essentially, the drop in elevation of the oil surface Δz was measured at several streamwise locations. The pressure gradient $\mathrm{d}p/\mathrm{d}x$ was then calculated from $\Delta z/\Delta x$ via the hydrostatic relationship. Precision of the individual measurements was about 0.05 mm which propagated to an estimated experimental uncertainty of 0.14 mm for Δz, comparable to the measurement in some cases (the percentage uncertainty of Δx was negligible). Fortunately, the determination of τ_w (or u_τ) is insensitive to the estimated experimental uncertainty in $\mathrm{d}p/\mathrm{d}x$ (McEligot 1985, figure 4).

The one-point technique suggested by McEligot (1984, 1985) was extended slightly and was applied to determine the wall shear stress. The wall sensor calibration was done essentially *in situ*. The one-point technique deduces the mean wall shear stress from the measured mean streamwise velocity U at a measured distance from the wall, via a turbulence model for the viscous layer (Huffman & Bradshaw 1972). This model accounts for the streamwise pressure gradient; as shown in figure 2, near $y^+ \approx 10$, it is relatively insensitive to the value of K_p. The turbulence model yields a mean velocity profile which is fit iteratively through the mean velocity measured at a point with dependence on the measured pressure gradient. McEligot (1984) presented the details including sensitivity to turbulence model and measurements, resulting experimental uncertainties and the Couette flow analysis upon which it was based. The turbulence models of McEligot & Bankston (1969), Huffman & Bradshaw (1972) and Kays & Crawford (1980) are all based on modifying the constant A^+ (in a van Driest representation of the mixing length) for agreement with experiments – and the functions $A^+\{K_p\}$ agree between them. For $y^+ < 10$ and $-K_p = 0.01$, the resulting mean velocity profile of Huffman & Bradshaw agreed with that of Kays & Crawford to within about 2 %; the corresponding difference in the deduced value of u_τ is then about 1 % between the two models. For the present data at $-K_p \approx 0.0083$, the DNS predictions of Mansour, Kim & Moin (1988) (with a slightly lower pressure gradient) are about 3 % below the curve of Huffman & Bradshaw in the region where it is adjusted to a data point. Suzuki & Kasagi (1992) have successfully employed

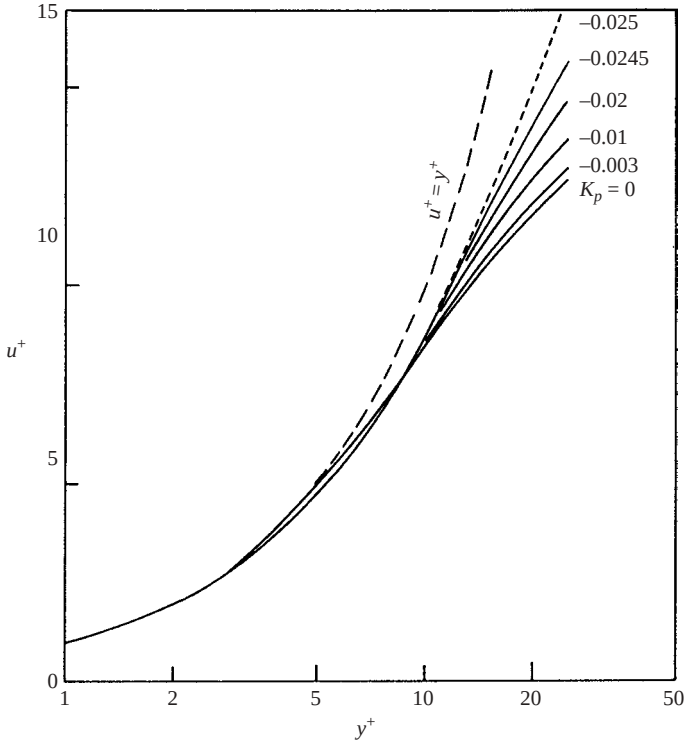

FIGURE 2. Mean velocity predictions using function $A\{K_p\}$ for the van Driest mixing length model (1956) as deduced by Huffman & Bradshaw (1972).

this technique in comparing hot-film measurements in a water channel to a DNS database.

For fully developed flows, the assumption that the convective terms are negligible in the governing momentum equation

$$u^+(\partial u^+/\partial x^+) + v^+(\partial u^+/\partial y^+) = -K_p + (\partial \tau^+/\partial y^+)$$

is ideally approached. However, for spatially accelerating flows, the relative magnitude of these terms depends on the applied pressure gradient and the distance y from the wall. To account for the convective terms, we adopted a suggestion of Finnicum & Hanratty (1988) based on earlier work of Julien *et al.* (1969) which gives the approximation

$$\tau^+\{y^+\} = (\tau\{y^+\}/\tau_w) = 1 + K_p y^+ \left[1 - (cf/(2y^+)) \int_0^{y^+} (u^+)^2 \, \mathrm{d}y^+\right].$$

The effect of the convective terms was evaluated for several accelerated flows of interest by conducting the calculations with and without the correction. For $y^+ \approx 10$ and less, typical results showed differences of 1.5 % or less for K_p and 0.5 % or less for u_τ. Since values with the cross-wire probe at y^+ near 10 are used to determine τ_w for calibration and for calculating wall coordinates, the inclusion of the convective terms led to no great change. Experimental uncertainties in the determination of the friction velocity by this method are of the order of 1 %, comparable to the sensitivity to the choice of turbulence model. With the cross-wire probe at $y^+ \approx 10$, it was away

Ramp angle (deg.)	K_p	$Re_{D,h}$	Re_s	K_v
		Streamwise accelerating flows		
2	−0.011	12 400	8300	1.6×10^{-6}
2	−0.02	8280	5600	2.4×10^{-6}
		'Fully developed' flows		
0	−0.0083	11 100	7400	6×10^{-9}
0	−0.011	8300	5600	5×10^{-9}

TABLE 1. Operating conditions.

from significant wall interaction but close enough that the uncertainty due to choice of a turbulence model was minimal.

As explained in the section above, during calibration of the wall sensor, the mean wall shear stress is determined by the one-point method as revised. The calibration data are extracted from normal measuring runs. For the fully developed conditions, measurements are available at four wall shear stress levels corresponding to runs at four flow rates (or pump speeds). Thus, the flow is turbulent with the same fluctuating field present during calibration as during application. Further details are provided by McEligot & Eckelmann (2003, Appendix B).

Although the temperature of the room was closely controlled by thermostats, there were slight variations from run to run during the overall period of the measuring program, say ± 0.1 K. During an individual run, the fluctuation was a few hundredths of a degree at most. Since the overheat ratio used for the wall sensor operation was relatively low (equivalent to about 10 K), a first-order temperature correction was developed. The approach is comparable to that suggested by Morrow & Kline (1971).

In data reduction, a subroutine is employed to apply a correction for the (small) difference between operating temperature and calibration temperature, to calculate the velocity across the sensor and, for the cross-wire probe, to apply a calibrated relation with the angular dependence to deduce the instantaneous velocity components. These time series of velocity components are integrated to yield the various mean statistics desired.

3. Results

The primary experimental results are the simultaneous measurements with the wall sensor for τ_w and the cross-wire probe for u and v. Velocity data were concentrated in the viscous sublayer at $y^+ \approx 5$, 7, 10, 15 and 25 (nominal values) plus the centreplane. Typically, 200 000 samples of each signal were acquired for the time series. Four sets of operating conditions were selected (table 1). This selection of conditions permits separating effects of K_p from Re_s and from K_v. For example, at one (approximately constant) Reynolds number there are data at two different values of K_p, and vice versa.

Mean turbulence statistics and additional mean velocity profile measurements are given by McEligot & Eckelmann (2003, tables 2 and 3). Results presented here are these mean statistics, probability density distributions, selected auto- and cross-correlations plus power spectra of the signals at $y^+ \approx 15$. This section presents those results with discussion as appropriate. Usually our presentation is in terms of wall coordinates, concentrating on the viscous layer.

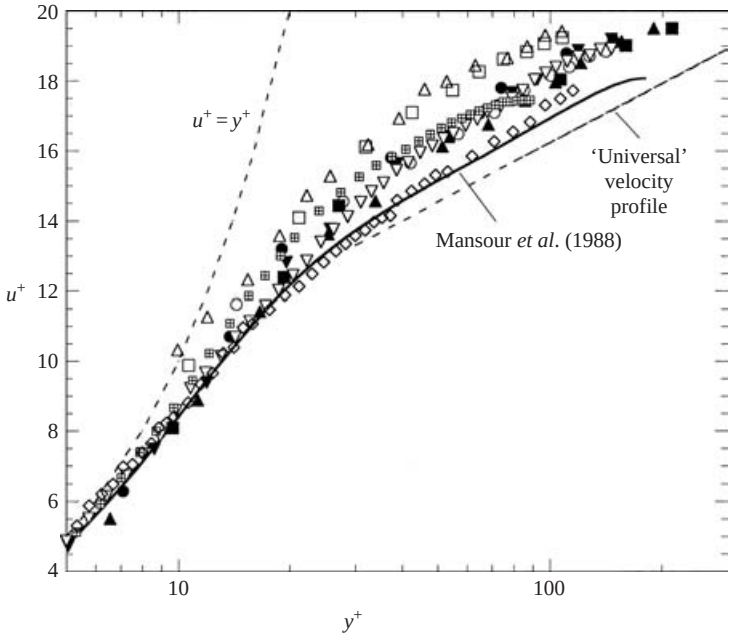

FIGURE 3. Streamwise mean velocity profile measurements ('fully developed': ▲, $K_p \approx -0.0083$; ▼, $K_p \approx -0.011$; laterally converging: ■, $K_p \approx -0.011$; ●, $K_p \approx -0.020$) as compared with other authors (—, Mansour *et al.* (1988), channel, $K_p \approx -0.006$; □, Senecal (1952), tube, $K_p \approx -0.018$; ○, Senecal (1952), tube, $K_p \approx -0.014$; Δ, Reynolds (1969), tube, $K_p \approx -0.018$; ∇, Durst *et al.* (1996), tube, $K_p \approx -0.014$; ⊞, Durst *et al.* (1998), channel, $K_p \approx -0.012$; ◇, Thiele & Eckelmann (1994), channel, $K_p \approx -0.006$).

Mean velocity profiles. The present streamwise mean velocity profiles along with other authors' data are presented in figure 3 in terms of wall coordinates. The present results are denoted by solid symbols, open symbols represent other author's data and the curve is from the direct numerical simulation by Mansour *et al.* (1988, hereinafter referred to as MKM88). These results cover an approximate range $0.006 < -K_p < 0.02$ and geometries of circular tubes, rectangular ducts and infinite parallel plates with Pitot tubes, thermal anemometry, laser velocimetry and DNS. The data confirm known trends; as K_p increases in magnitude, the curves $u^+\{y^+\}$ also have higher values away from the wall (Patel 1965). This observation is one effect of a streamwise pressure gradient on mean turbulence structure. It corresponds to a thickening (in terms of y^+) of the layer dominated by viscous effects as in the mixing-length wall models of McEligot *et al.* (1966), Launder & Jones (1969), Huffman & Bradshaw (1972) and others. The trend is also predicted by the direct numerical simulations of Spalart (1986). Comparable data have been obtained by Jones & Launder (1972) and Loyd, Moffat & Kays (1970) for converging (sink-like) flows, by Shehata & McEligot (1998) for strongly heated gas flows in tubes and in turbulent flows with drag reduction by polymer additives (Berman 1978; Harder & Tiederman 1989).

In figure 3, results for the lowest pressure gradients (Thiele & Eckelmann (1994) – open diamonds, MKM88) still show slight effects compared to the asymptotic 'universal velocity profile' for high Reynolds numbers or low pressure gradient conditions. The present data with larger values of $-K_p$ show larger differences.

The highest values of $-K_p$ are those of Senecal (1952) and Reynolds (1969) from circular tubes at $Re \approx 3000$ ($K_p \approx -0.018$) and the present data at $K_p \approx -0.02$ for laterally converging or accelerating flow. The tube results can be higher for a couple reasons. First, y_c^+ is only about 110 for these experiments, so influences from the far wall and 'side' walls are likely. Secondly, for the present accelerating flow, the convective terms in the momentum equation can become important as y^+ increases, so the distribution of $\tau^+\{y^+\}$ would be equivalent to a fully developed flow that has a lower value of $-K_p$. The second effect can also be seen in the present data by comparing the fully developed run at $-K_p \approx 0.011$ (inverted solid triangle) and the accelerated run with approximately the same pressure gradient (solid squares); at the larger values of y^+, mean velocities for the accelerated run are slightly lower than the fully developed one. These trends are essentially as expected when we consider the differences in geometries and in flow development.

The deduced values of the transverse mean velocity V^+ for the viscous layer and the centreplane are tabulated by McEligot & Eckelmann (2003, table 2). These data can be subject to a variety of difficulties. The calculation of $\tilde{v}$ from cross-wire probe signals involves determining the small difference between two much larger signals. (For a fully developed flow, V is ideally zero and consequently percentage experimental uncertainties are infinite.) In a fully developed flow in the same oil channel, Randolph (1987) found that, as his cross-wire probe approached the wall, the measurements yielded flow angles which were not parallel to the wall – a possible indication of wall–probe interaction. Moin & Spalart (1988) modelled the behaviour of a typical cross-wire probe via direct numerical simulations of a turbulent flow; they found that neglecting the spanwise component w led to larger errors in v than in u and the separation of the two films can have strong effects. Moin & Spalart did not present calculations of the expected measured value for the mean $V^+\{y^+\}$, but, in general, the predicted errors increased as y^+ approached zero with dependence on w and the calibration relations employed.

Other investigators have arbitrarily adjusted their sensor angles to force V to be zero. For a laterally converging flow, V is not identically zero so we carry the values actually deduced (and look for relative effects at the same locations). The mean values $V\{y^+\}$ are all towards the wall except centreplane values for the fully developed flows. The largest values appear at $y^+ \approx 7$ to 10 and then the magnitudes decrease as y^+ increases. However, they are generally less than about 5 % of the value of U at the same y^+. Although there are differences between the values of $V^+\{y^+\}$ for the various runs, there is no clear trend as K_p varies, and the difference at a given y^+ is generally within the experimental uncertainty.

Root mean square fluctuations. The normalized values of the r.m.s. velocity components are plotted in figure 4. In these figures and the remaining ones, results are presented only for channel flows.

Although the percentage experimental uncertainty of the mean normal component is infinite for an ideal fully developed flow, the uncertainty in r.m.s. fluctuations can be small enough to permit meaningful measurements. The experimental uncertainty in v' (or u') is determined by random uncertainties (Metzger 2002) whereas bias error plus random uncertainties contribute to the mean value. In the present experiment, these random uncertainties come primarily from electronic noise of the anemometer system, some noise in one amplifier and rounding error in the analogue-to-digital conversion. These effects are reduced in the results by the precisions of the suppression voltages which correspond approximately to the mean signals from the sensors.

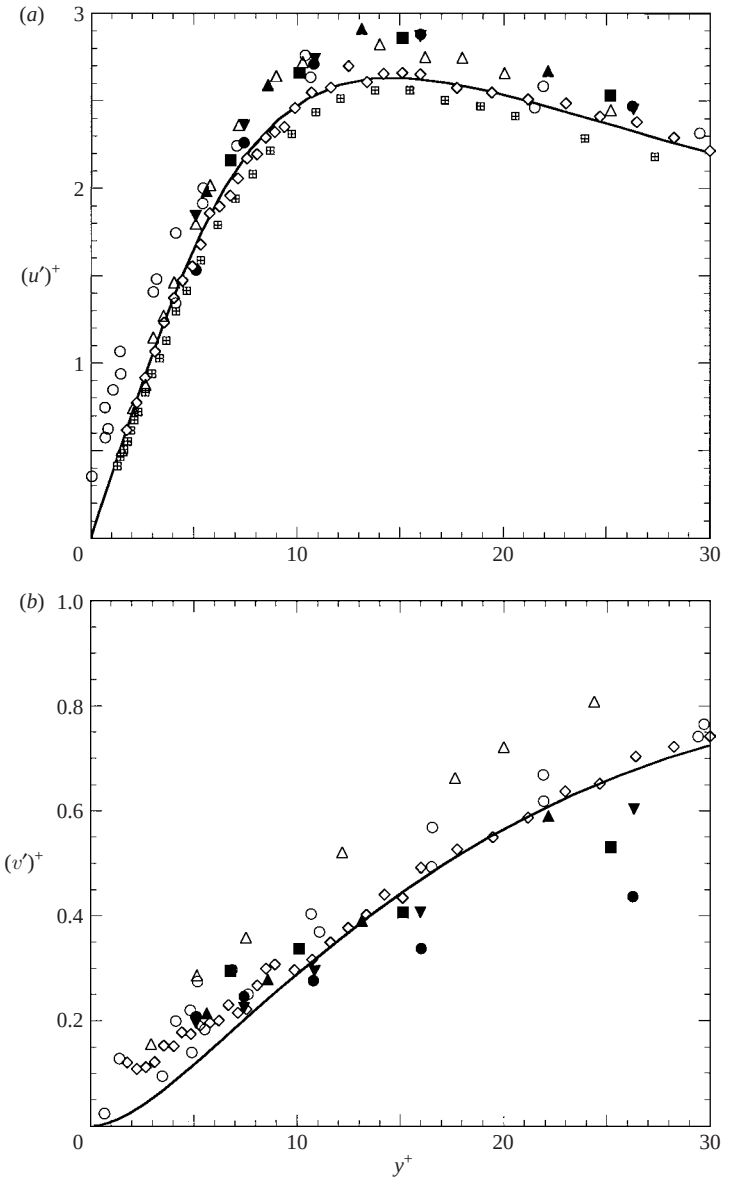

FIGURE 4. Root mean square values of velocity component fluctuations as compared with other authors, (*a*) streamwise and (*b*) wall-normal. (Symbols as in figure 3 plus Δ, Kreplin & Eckelmann (1979), channel, $K_p \approx -0.006$ and ○, Niederschulte *et al.* (1990), channel, $K_p \approx -0.006$).

The Disa 55M01 anemometer system was designed for low noise; Klewicki (personal communication, 2004) indicates that the noise in the raw signal is typically between one and three mv. The propagation of uncertainties leads to estimated uncertainties of the order of 0.2 % or less for u' and 0.8 % to 1.5 % for v' within the viscous layer in the run at $K_p \approx -0.0083$, a fully developed condition. In the accelerated flow at $K_p \approx -0.020$, the comparable estimates are 0.22 % and less for u' and 1.2 % to 1.9 % for v'. For the comparisons in terms of wall coordinates, the estimated uncertainly in

u_τ is about 1 % and the uncertainty in y^+ varies from about 1 % to 3 % depending on the distance from the surface.

Comparisons are to the hot-film data of Eckelmann (Kreplin & Eckelmann 1979*a–c*), the LDV measurements of Niederschulte, Adrian & Hanratty (1990) and Thiele & Eckelmann (1994) and the DNS of MKM88, all for fully developed flows at relatively low $-K_p$. However, the data shown for Durst *et al.* (1998) for the streamwise component are at $-K_p \approx 0.012$, significantly higher than most of the other fully developed flows. For $(u')^+$, the present fully developed runs (solid triangles) agree well with hot film data of Eckelmann (1974) in the same channel and the LDV measurements of Niederschulte *et al.* and show fair agreement with the LDV measurements of Thiele & Eckelmann and Durst *et al.* plus the DNS results. The maximum value approaches 3 at y^+ near 15, in agreement with the data of Eckelmann (1974) and others.

Conceptually, the distribution of $(u')^+$ may be affected by Reynolds number or pressure gradient or both. Eckelmann compared his data at two Reynolds numbers, corresponding to our two fully developed conditions. When non-dimensionalized with wall coordinates (his figure 13) the data collapsed, i.e. there was no apparent effect of Reynolds number. This observation is consistent with the results of MKM99, who showed only a slight variation of the $(u')^+$ distribution over larger ranges of (low) Reynolds numbers and therefore of $-K_p$. From the data of Fernholz & Finley (1996) and their own, Metzger & Klewicki (2001; Metzger 2002) suggest that there is only a gradual increase of $(u'_{max})^+$ with Reynolds number, a factor of about 1.4 over four orders-of-magnitude. In the present experiment, the difference between the lowest and highest Reynolds numbers is only about 33 %, so no significant effect of Reynolds number is expected. However, the measured K_p changes by a factor of about 2.5 so the question becomes whether it induces any significant modification of the $(u')^+$ profile. Our figure 4*a* for u', using comparable wall scaling, shows the answer to be negative. That is, for these measures of the turbulence structure, there appears to be no important effect of the streamwise pressure gradient on the streamwise fluctuation $(u')^+$.

Earlier, Reichardt (1938; Schlichting 1968), Durst *et al.* (1995), MKM99 and others have shown that the mean value for $(v')^+$ should be less than that for $(u')^+$ and its peak should occur further from the wall than for $(u')^+$. Durst *et al.* show $(v')^+$ of about 0.8 to unity occurring near $y^+ \approx 100$. Therefore, in the viscous layer, $(v')^+$ increases monotonically and has a lower magnitude than $(u')^+$.

In figure 4(*b*) the present measurements of v' are compared to those presented by Kreplin & Eckelmann (1979*c*) with a hot-film cross-wire probe, Niederschulte *et al.* (1990) by two-component LDV and by Thiele & Eckelmann (1994) with a customized two-component LDV as well as the DNS predictions of MKM88 at $Re_\tau \approx 180$. Their studies were all for K_p of the order of -0.006 and fully developed low-Reynolds-number channel flow ($9800 < Re_{Dh} < 11\,800$). The estimated experimental uncertainties of the present data are of the size of the symbols or smaller. The non-dimensional length and spacing of the sensors for the data of Brodkey *et al.* (1974) reported by Kreplin & Eckelmann ($l_s+ \approx s^+ \approx 1.8$) were comparable to the present cross-wire probe at $Re_{Dh} \approx 8300$; Niederschulte *et al.* had a smaller diameter at $d^+ \approx 0.26$, but the length of their measuring control volume was $l^+ \approx 1.8$ which is comparable to the spacing of the hot-film sensors in the present study. In the DNS calculations, the grid spacing was $\Delta x^+ \approx 12$, $\Delta y^+ \approx 1.0$ and $\Delta z^+ \approx 7$ at $y^+ \approx 5$ [KMM; MKM88; Mansour 2001]; the normal spacing Δy^+ decreased as the wall was approached and increased at larger distances. The optical arrangement of the

LDV of Thiele & Eckelmann reduced the size of its measuring control volume to $d^+ \approx l^+ \approx 0.53$ so they tended to have the best spatial resolution of the investigations shown here. The spatial resolution of the measurements was considerably better than the DNS predictions in the streamwise and spanwise directions. The non-dimensional sampling durations ($2TU_c/s$) of these studies were 1900 for Niederschulte *et al.*, 5160 for Brodkey *et al.*, 1040 (central region) to 9300 (near wall) by Thiele & Eckelmann and 5550 to 7400 for the present data.

The present data for fully developed flow at the lowest pressure gradient (solid upright triangles) agree closely with the simulations of MKM88 and the measurements of Thiele & Eckelmann. For y^+ less than 10 or so, most of the previous data are seen to be higher that the DNS predictions; the data of Niederschulte *et al.* show considerable scatter for y^+ less than 5, but their average trend corresponds to the results of Thiele & Eckelmann and the present study. The present data are consistent with the observation that the DNS results appear to be low in this region. In the current study, the raw data for the mean normal velocity were slightly negative near the wall (McEligot & Eckelmann 2003) so this apparent inflow could carry slightly higher values of v' into this region; whether this situation occurred in the other studies is not clear. For y^+ greater than about 7, the present data for low K_p (upright triangles) agree with the DNS predications as well or better than the others do.

The predictions from the DNS of sink flows by Spalart (1986), the analysis of Finnicum & Hanratty and the duct flows by MKM99 indicate that increasing the streamwise pressure gradient should produce observable effects on $(v')^+$ in the viscous layer – but this variation had not been confirmed experimentally. The idea that $v'\{y^+\}/u_\tau$ may not be independent of streamwise pressure gradients is tested by our figure 4(*b*) as well as being addressed in the analysis of Finnicum & Hanratty (1988, figure 7) and the direct simulations of Spalart (1986, personal communication 1990). A trend is seen towards a reduction in $v'\{y^+\}/u_\tau$ with increase in the magnitude of $-K_p$, more favourable pressure gradients. The question is how large is the effect?

To examine the effects of increased streamwise pressure gradient or acceleration on $(v')^+$, it is convenient to compare the data at the lowest $-K_p$ (upright triangles) to those at the highest (circles). For these two runs, the measured $-K_p$ increases from 0.008 to 0.020, K_v increases from near zero to 2.4×10^{-6} and Re_{Dh} decreases from 11 100 to 8280. Within the viscous layer, we see a relative reduction in $(v')^+$ as y^+ and the streamwise pressure gradient increase. At $y^+ \approx 25$, this reduction relative to MKM88 is about 36 %. The DNS predictions of MKM99 cover a range of $-K_p$ from about 0.0056 to 0.0017 as Re_{Dh} is increased from about 11 200 to 45 000. Their overall change in $(v')^+$ was about 13 % whereas for the increase of $-K_p$ from 0.0017 to 0.0026, their reduction was only about 1 %. From comparison to their results, it appears that the reduction of $(v')^+$ in the present data may be a consequence of increased pressure gradient (or related acceleration) in addition to the change in Reynolds number. Since the converging run at $-K_p \approx 0.020$ in the present experiment was at approximately the same Reynolds number as a fully developed run ($Re_{Dh} \approx 8300$, $-K_p \approx 0.011$, inverted triangles), the phenomena can be separated to some extent. With the Reynolds number approximately constant, the reduction in $(v')^+$ is seen to be about 28 %. Finnicum & Hanratty predict a drop of about 40 % from $K_u = 0$ to 2.0×10^{-6} while Spalart's results suggest about 25 % for K_u increasing from 1.5×10^{-6} to 2.5×10^{-6}, both at $y^+ \approx 25$. Our data essentially confirm the trends of these predictions.

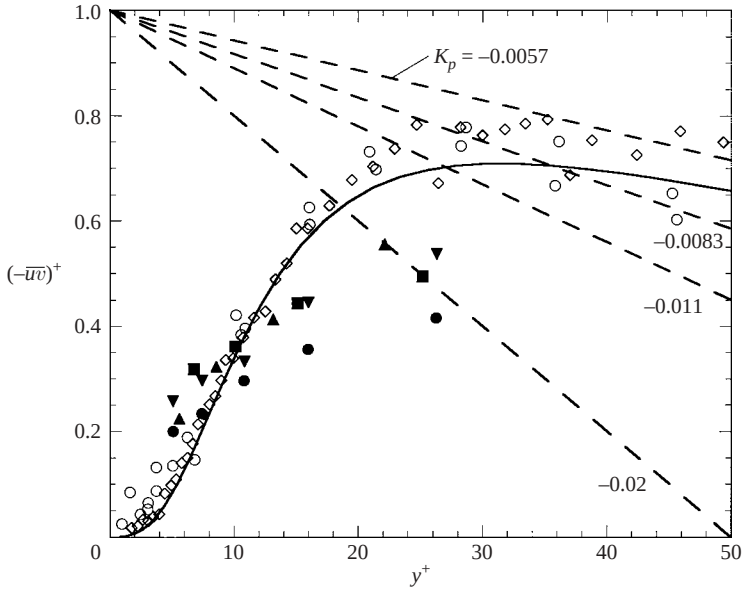

FIGURE 5. Variation of Reynolds shear stresses compared to other authors and to asymptotes (dashed) for fully developed flow (symbols as in figures 3 and 4).

Reynolds shear stress ($=-\rho\overline{uv}$ where the overbar denotes the time mean value of the product of the fluctuations u and v). With the dimensions of the channel and the flow rates yielding centreline values of y^+ in the range of 140 to 210 in the present experiment, the total shear stress varies observably across the viscous layer. Therefore, the popular constant shear-layer approximation is not valid, even for the fully developed flows. For the effect in the viscous layer to be less than about 5 %, the centreplane value y_c^+ (or Re_τ) should be about 600 or more.

As noted above, for fully developed flow, the total shear stress variation is given as $\tau^+\{y^+\} = (\tau\{y^+\}/\tau_w) = 1 + K_p y^+$ (with accelerating flows, at large y^+, the convective terms counter this reduction somewhat). At the wall $u = v = 0$, so $\overline{uv}$ is likewise zero there. Since

$$\tau\{y\} = \mu(\partial U/\partial y) - \rho\overline{uv} \quad \text{or} \quad \tau^+ = (\partial U^+/\partial y^+) - (\overline{uv})^+,$$

the Reynolds shear stress increases with y in the viscous layer, approaching the total shear stress relation as the turbulent transport becomes dominant relative to viscous effects. (The symbol μ represents the absolute viscosity.) That is, for fully developed flows, the quantity $1 + K_p y^+$ forms an asymptote for $(\overline{uv})^+$. Consequently, $(\overline{uv})^+$ should approach a peak at a magnitude that decreases as $-K_p$ increases. For accelerating flows the comparable peak will have a different value and location.

The present results are shown in figure 5 along with those for the fully-developed flows at $K_p \approx -0.006$ by Niederschulte *et al.*, by Thiele & Eckelmann and by MKM88. Approximate asymptotic values for $\tau\{y^+\}$ versus K_p in the viscous layer are provided as dashed lines. The predicted curve from MKM88 can be seen to be approaching its asymptotic curve for $-K_p \approx 0.0057$ – and the measurements of Thiele & Eckelmann and of Niederschulte *et al.*, are in approximate agreement. The data for the fully-developed runs in the present study (solid triangles) are at higher $-K_p$ and therefore are lower, approaching their respective (lower) asymptotes. The measurements for our accelerating flow with the highest $-K_p$ (solid circles) have the

lowest magnitudes of $(\overline{uv})^+$ in the viscous layer; their trend is towards a curve of $\tau^+\{y^+\}$ (accounting for convective terms) at larger values of y^+ than given by the fully developed asymptote shown.

The measurements of v' (and therefore $\overline{v^2}$) and $\overline{uv}$ permit examination of the model of Panton & Linebarger (1974) for wall pressure spectra. A key hypothesis of Panton & Linebarger is that the intensity of the normal velocity component scales with the Reynolds shear stress and normalized wall distance, i.e. $(\overline{v}^2/\overline{uv}) = fn\{y^+\}$, but does not depend on pressure gradient. McEligot & Eckelmann (2003) employed the present data to test this hypothesis by comparing results for the quotient $(\overline{v}^2/\overline{uv})$. In the viscous layer, this quantity varies approximately linearly with y^+. For the two fully developed runs, the values decrease slightly as $-K_p$ increases. For the accelerating runs, the reduction is greater as y^+ increases and the slope is less. The present data indicate that for viscous layers, an improvement in the hypothesis of Panton & Linebarger may be warranted.

Probability density distributions. The time series have been analysed to develop probability density distributions for instantaneous streamwise and normal velocities and their product. The two extreme runs are examined, i.e. data from the accelerating run at $K_p \approx -0.02$ and the run at $K_p \approx -0.008$, the higher-velocity fully developed case. In order to compare results directly, they are presented in terms of wall coordinates and the fraction of total samples (200 000 in these runs). Thus, for the streamwise velocity a probability density distribution $N'\{\tilde{u}^+\}$ is defined as

$$\int_0^\infty N'\{\tilde{u}^+\}\,\mathrm{d}u^+ = \sum N'\{\tilde{u}^+\}\Delta u^+ = 1.$$

Here, the symbol $\tilde{u}^+$ represents an instantaneous total value of the streamwise component in wall coordinates. The units of $N'\{\tilde{u}^+\}$ are essentially the fraction of samples per unit of $\tilde{u}^+$. The expected maximum range of $\tilde{u}^+$ was divided into 100 intervals $\Delta\tilde{u}^+$. The distributions $N'\{\tilde{v}^+\}$ and $N'\{(\tilde{u}\tilde{v})^+\}$ were formed in a like manner with the exception that their differing ranges led to different interval widths (e.g. $\Delta\tilde{v}^+$).

When plotted versus linear coordinates (not shown), the results for $N'\{\tilde{u}^+\}$ at $K_p \approx -0.008$ are consistent with those presented by Eckelmann (1974) in his figure 10 for his highest flow rate. The most accelerated run ($K_p \approx -0.02$) shows the same trends and magnitudes as the fully developed run ($K_p \approx -0.008$). Thus, we may conclude that there is no significant effect of streamwise pressure gradient on $N'\{\tilde{u}^+\}$ from slight to strong values.

The probability density distributions of the normal velocity $\tilde{v}^+$ for the fully developed case demonstrate the same behaviour as presented in their figure 11 by Brodkey *et al.* (1974), when plotted versus linear coordinates (not shown). Near the wall, the distributions are narrower and therefore have higher peak values than further from the wall. The most probable values of $\tilde{v}^+$ are slightly less than the mean, i.e. they represent small velocities towards the wall. Magnitudes of $\tilde{v}^+$ much greater and much less than the probable value are evident; for $y^+ \approx 22.2$, it is seen that the maximum value of $|\tilde{v}^+|$ is greater than 2 (while the mean is ideally zero).

In order to examine the maximum excursions in $\tilde{v}^+$, the probability density distributions are presented in semi-logarithmic coordinates in figure 6 (solid symbols are for the laterally converging case and open symbols are for the fully developed situation). The general trends of both sets are the same: the peak $N'\{\tilde{v}^+\}$ is reduced as $N'\{\tilde{v}^+\}$ broadens with an increase in y^+. Maximum values of $|\tilde{v}^+|$ approach 4 and

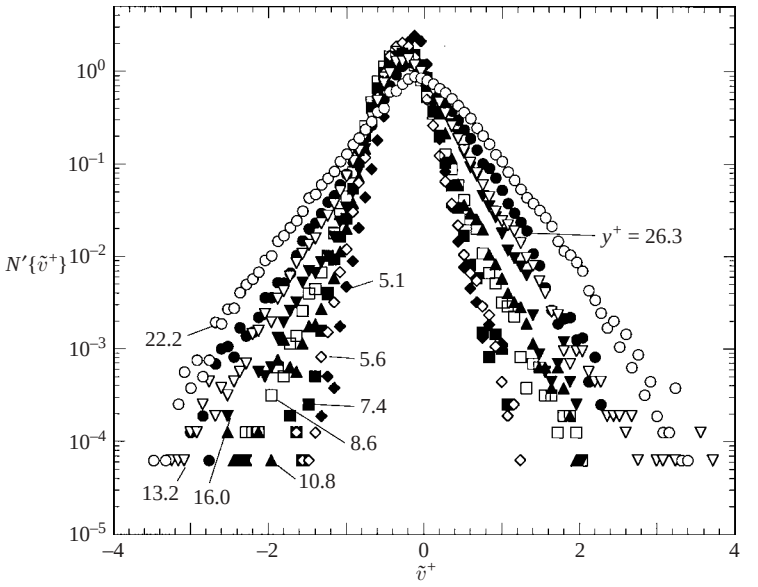

FIGURE 6. Probability density distributions of instantaneous wall-normal velocity (open symbols: 'fully developed', $K_p \approx -0.0083$; solid symbols: laterally converging flow, $K_p \approx -0.020$). $\Delta\tilde{v}^+ = 0.08$.

occur for the fully developed run at $y^+ \approx 22$. The approximately exponential decrease of $N'\{\tilde{v}^+\}$ is observed for all locations in both sets of experimental conditions. For the laterally converging flow the first location ($y^+ \approx 5.1$) is closer to the wall than in the fully developed case and its peak $N'\{\tilde{v}^+\}$ is accordingly higher. An exponential decrease of values away from the most probable value is seen to very low values of $N'\{\tilde{v}^+\}$ (i.e. very few counts). For $y^+ \approx 26.3$, towards the edge of the viscous layer, we see values of $\tilde{v}^+$ greater than 2 and as low as -3. The large negative velocities could correspond to energetic 'sweeps' towards the wall and the large positive ones would represent 'ejections' or 'outward interactions'. For a fully developed flow in the same channel, Brodkey *et al.* (1974) concluded via quadrant-splitting analyses that the outward flow at $y^+ \approx 30$ was predominantly due to ejections rather than outward interactions. In contrast to the fully developed flow, near the wall, the most probable values of $\tilde{v}^+$ (i.e. $\tilde{v}^+$ at the maximum of $N'\{\tilde{v}^+\}$) are greater than the mean; further away, the most probable values are less than the mean, in agreement with the trends of the fully developed flow.

The probability density distributions for the normal velocity are affected by the laterally converging flow or streamwise pressure gradient. In addition to the near-wall differences mentioned above, it appears that towards the outer edge of the viscous layer, the range of values of $\tilde{v}^+$ is broader for the fully developed case than the accelerated one (e.g. $y^+ \approx 22.2$ in the fully developed case compared to the larger $y^+ \approx 26.3$ in the accelerated case). Since the locations in the two runs are not at the same values of y^+, we cannot make direct comparisons. We quantified the differences in the two runs in two ways. From figure 6 one can plot the variation of the apparent peak $N'\{\tilde{v}^+\}$ versus y^+ for both cases or a measure of the breadth of $N'\{\tilde{v}^+\}$ can be evaluated; an appropriate quantity is the width at the level $N'\{\tilde{v}^+\} = 0.01$ $N'_{max}\{\tilde{v}^+\}$ for each location (McEligot & Eckelmann 2003). The two approaches are complementary. Near the wall, one cannot discriminate between the results of the

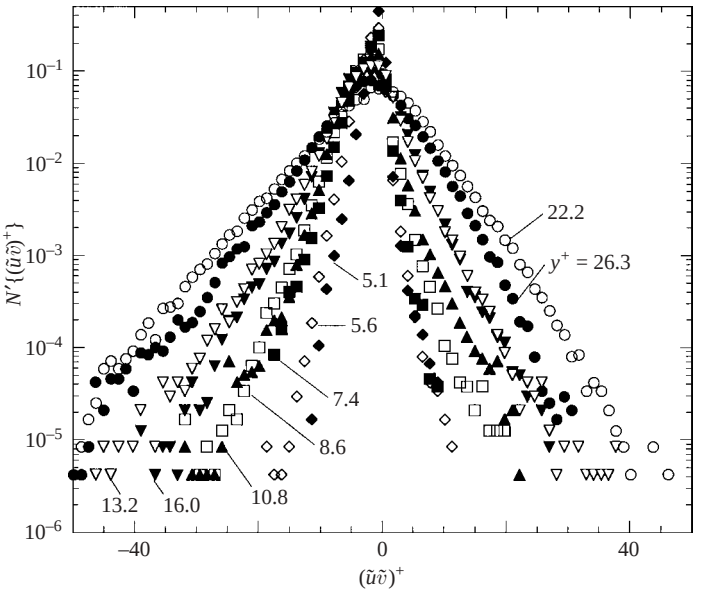

FIGURE 7. Probability density distributions of product of instantaneous streamwise and instantaneous normal velocities (symbols as in figure 6). $\Delta(\tilde{u}\tilde{v})^+ = 1.2$.

two cases. However, for $y^+ > 12$, the peak value is higher for the accelerated case and it is narrower than one might expect based on the fully developed distributions. That is, at a given location near the edge of the viscous layer, the range of values of $\tilde{v}^+$ observed for $K_p \approx -0.02$ is significantly smaller. Since $N'\{\tilde{u}^+\}$ apparently was not significantly affected, this observation implies that the range of angles of the instantaneous velocity vector (Kreplin & Eckelmann, 1979*b*) would be less.

The probability density distributions of $(\tilde{u}\tilde{v})^+$ (figure 7) generally show the same trends as $N'\{\tilde{v}^+\}$. Since this quantity is formed as the product of the instantaneous total values of $\tilde{u}$ and $\tilde{v}$ (rather than the fluctuations about their means), the mean value is given by $(U^+V^+ + (\overline{uv})^+)$ for the accelerated run. The mean product of the fluctuations $(\overline{uv})^+$ ranges between zero and negative unity and U^+V^+ is about one to two. So it is obvious that excursions of $(\tilde{u}\tilde{v})^+$, from which the Reynolds shear stress is derived, are much greater than the mean of $(\tilde{u}\tilde{v})^+$, particularly near the edge of the viscous layer (e.g. 50 versus 2). Again, the variation of $N'\{(\tilde{u}\tilde{v})^+\}$ in the lower decades of its magnitude is approximately exponential. And again we see that, in the outer part of the viscous layer, the width is narrower for the laterally converging case than for fully developed flow.

Probability density distributions of uv (the product of the fluctuations) at $y^+ \approx 30$ are presented by Willmarth & Lu (1972) in their figure 14 and at $3.4 < y^+ < 195$ by Brodkey *et al.* (1974) in their figure 9. Both studies showed the most probable values of uv to be near zero and at values of uv greater than $\overline{uv}$, which is negative. Willmarth & Lu suggest that the peak at uv near zero corresponds to the fact that uv is relatively quiescent much of the time and that the long tail for $uv < 0$ is a result of the spiky nature of Reynolds-shear-stress contributions during bursting events. Brodkey *et al.* found large negative values of uv near the edge of the viscous layer to be mostly due to ejections while near the wall they usually represented sweeps.

For our fully developed run, comparable probability density distributions were observed for the quantity $(\tilde{u}\tilde{v})^+$. The value of $(\tilde{u}\tilde{v})^+$ at $N'_{max}\{(\tilde{u}\tilde{v})^+\}$ was likewise

greater than the mean of $(\tilde{u}\tilde{v})^+$, except for $y^+ \approx 5.6$ where they were approximately equal. Some changes are evident for the accelerated case. Near the wall, the value of $(\tilde{u}\tilde{v})^+$ for the peak $N'\{(\tilde{u}\tilde{v})^+\}$ was about the same as the mean of $(\tilde{u}\tilde{v})^+$; then for $y^+ \approx 7.4$ and 10.8 it was larger (more positive), as for the fully developed run. However, towards the edge of the viscous layer, this relative trend decreased, with the value of $(\tilde{u}\tilde{v})^+$ for the peak $N'\{(\tilde{u}\tilde{v})^+\}$ being about the same as the mean of $(\tilde{u}\tilde{v})^+$ at $y^+ \approx 16$, and then at $y^+ \approx 26.3$ the trend reversed with the value of $(\tilde{u}\tilde{v})^+$ for the peak $N'\{(\tilde{u}\tilde{v})^+\}$ becoming less than the mean of $(\tilde{u}\tilde{v})^+$.

The logarithmic scale of the ordinate allows better examination of the distributions of extreme values than a linear presentation does. The 'tails' of the distributions at $N'\{(\tilde{u}\tilde{v})^+\} < \sim 0.01$ appear generally non-symmetric relative to the means. These extremes represent the larger values of $|\tilde{u}\tilde{v}|$, more 'energetic'. The values of $N'\{(\tilde{u}\tilde{v})^+\}$ are greater for a given negative value of $(\tilde{u}\tilde{v})^+$ than for the equivalent positive value. Negative values of $(\tilde{u}\tilde{v})^+$ correspond to momentum transport by sweeps and ejections while positive ones are from wallward and outward interactions. This observation is another indication that large values of $|\tilde{u}\tilde{v}|$ are more likely to come from sweeps and ejections than from interactions.

The $N'\{(\tilde{u}\tilde{v})^+\}$ distributions for $y^+ \approx 13.2$ and 22.2 in the fully developed run are wider than for $y^+ \approx 16.0$ and 26.3, respectively, in the accelerated run. (This result corresponds to an earlier comment concerning the $N'\{\tilde{v}^+\}$ distribution.) Consequently, we may conclude that another effect of a strong streamwise pressure gradient is to reduce the magnitudes of the largest values of $|(\tilde{u}\tilde{v})^+|$ in the outer part of the viscous layer – and this reduction is smaller owing to the smaller maximum value of $|\tilde{v}^+|$. The lower value of the Reynolds shear stress $(\overline{uv})^+$ for $K_p \approx -0.02$ has already been shown in figure 5.

In summary, the probability density distributions for $\tilde{u}^+$ show no significant effects of the streamwise pressure gradient, while those for $\tilde{v}^+$ and $(\tilde{u}\tilde{v})^+$ do so near the edge of the viscous layer. For the converging flow, the transport of momentum is reduced there compared to the fully developed case, as demonstrated by the comparison for $y^+ \approx 13.2$ and 22.2 (fully developed) to those of $y^+ \approx 16.0$ and 26.3 (converging) and by figure 5. This observation implies lessening of the vigour of the ejections as confirmed by the trends of $N'\{\tilde{v}^+\}$ as well.

Skewness and flatness. The skewness and flatness factors were calculated from the time series for u and v to quantify some aspects of the probability density distributions. The present data for skewness and flatness factors, S and F, are compared to those of other authors in figures 8 and 9.

Thiele & Eckelmann (1994) noted that, 'Whereas smooth curves result for the u component in all investigations, the skewness factors of the normal fluctuations are characterized by considerable scatter in the results of all authors' (those included in their comparisons). For the present data, we could generally connect the plotted points with smooth curves for each individual run, despite the magnitudes of the estimated experimental uncertainties. Unfortunately, the other authors have not presented quantitative estimates of their uncertainties. Our estimates showed the experimental uncertainties in S_u and F_u to be about an order-of-magnitude smaller than those for S_v and F_v; the uncertainties in S_u and F_u are about the size of the symbols in our graphs (or less). For S_v our uncertainty estimates varied from about 0.08 to 0.19 for the runs with the highest and lowest pressure gradients; these estimates are shown on figure 9*a* by vertical brackets. Thiele & Eckelmann suggest that measurement uncertainties have greater effects on the calculation of higher

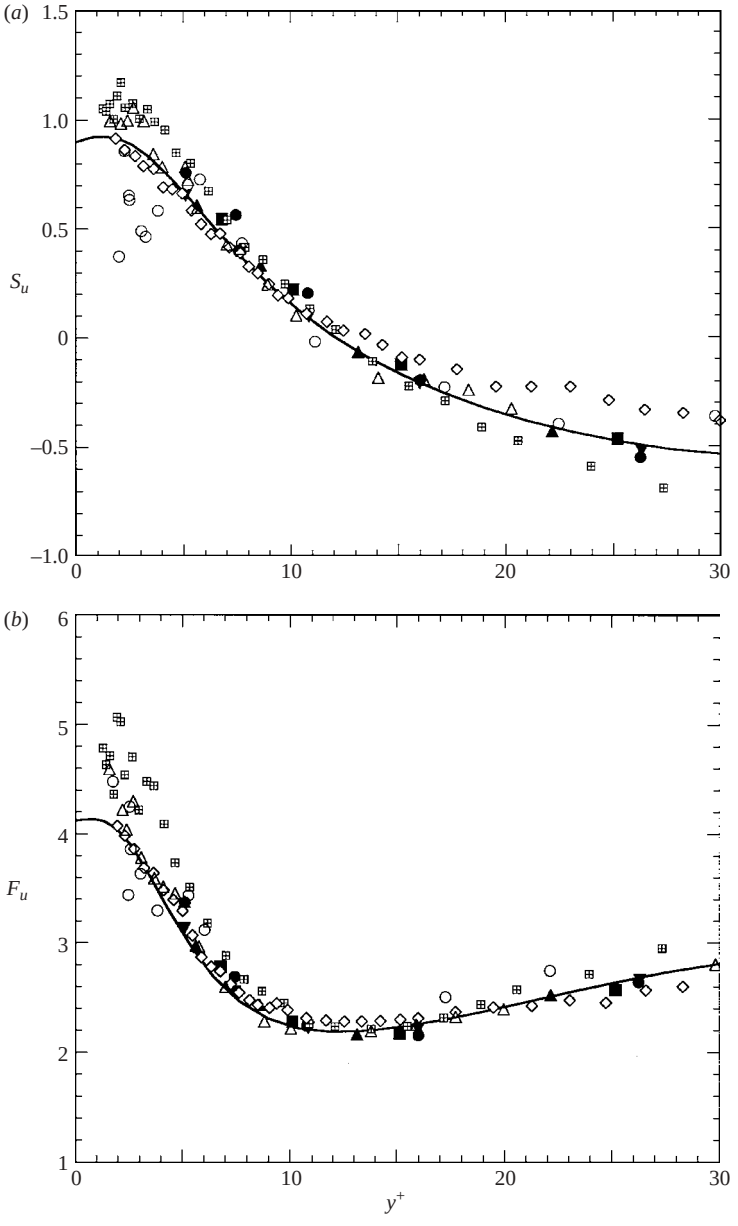

FIGURE 8. Distributions of (*a*) skewness and (*b*) flatness factors of streamwise velocity fluctuations (—, Moser *et al.* (1999) web site; other symbols as in figures 3 and 4).

moments when the probability density distribution is narrow – as it is for the normal component. Also, for their boundary layers, Klewicki & Falco (1990) demonstrated that considerably more sampling time was required for convergence of skewness and flatness factors than for mean and root-mean-square determinations.

Most data for the skewness factors of the streamwise fluctuations S_u agree closely with the predictions of MKM99, with the present measurements for the fully developed runs (solid triangles) agreeing as well or better than the others (figure 8*a*). We can discern a slight effect of pressure gradient, with S_u being higher near the wall

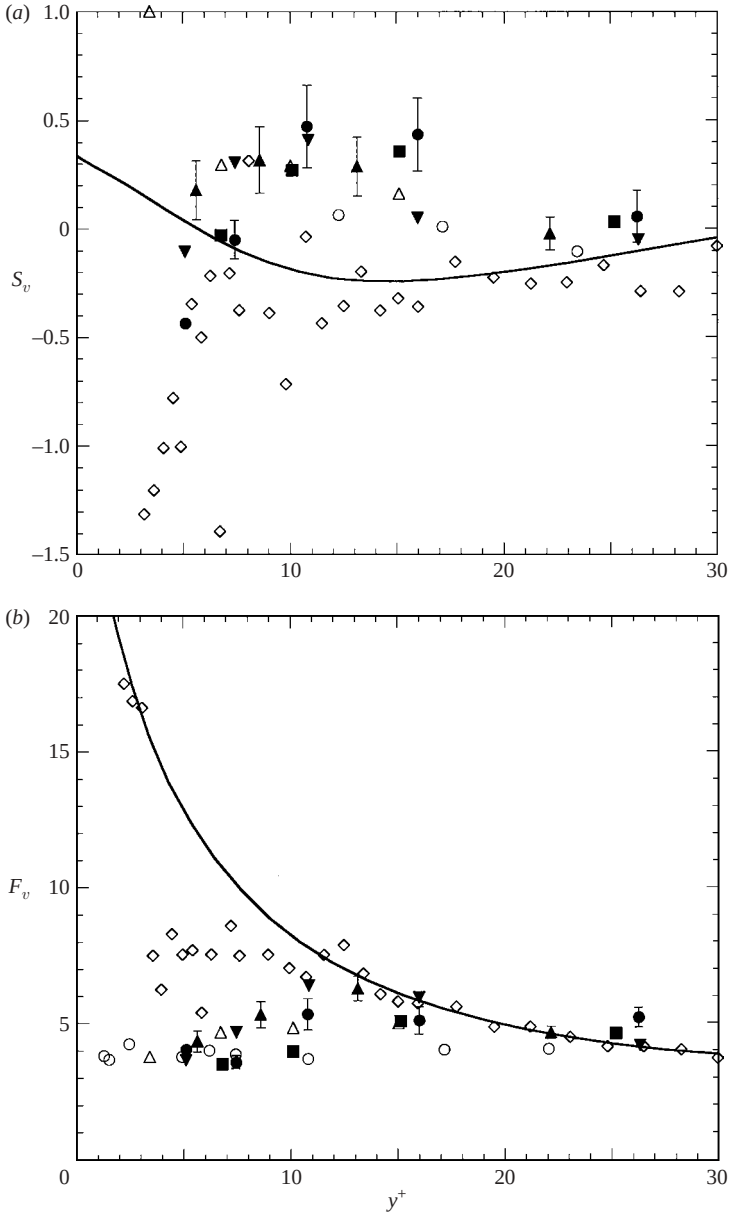

FIGURE 9. Distributions of (*a*) skewness and (*b*) flatness factors of wall-normal velocity fluctuations (—, Moser *et al.* (1999) web site; other symbols as in figures 3 and 4).

and lower for $y^+ > 20$ or so. These trends are consistent with the measurements by Durst *et al.* (1998) at $-K_p \approx 0.012$, a moderate pressure gradient.

As with the skewness factor, the measurements of the flatness factor for streamwise fluctuations F_u (figure 8*b*) agree closely with the MKM99 predictions, and the present data are as close or closer than the others. The pressure gradient appears to induce a slight increase for low y^+ and a decrease for higher distances, but the effects observed are of the order of the uncertainty estimates (approximately the size of the symbols) so they are not definitive. The data of Durst *et al.* (1998) at $-K_p \approx 0.012$ show

greater effects, but greater scatter and trend in the opposite direction for y^+ greater than about 20.

For S_v, the present measurements and some others disagree with the DNS predictions for y^+ less than 20 (figure 9*a*). The present measurements show consistent trends and possibly some variation with pressure gradient: S_v increases from negative values at low y^+ to maxima at $y^+ \approx 10$–15 and then decreases to near zero. Our data are in approximate agreement with those of Niederschulte *et al.* (1990) and Kreplin & Eckelmann (1979*c*), but differ somewhat from the experiment of Thiele & Eckelmann (1994). For $6 < y^+ < 20$, the present data yield a positive skewness factor while MKM99 predict it to be negative; further, the decreasing trend for $y^+ < 10$ is opposite to the trend predicted by DNS. Above y^+ of about 20, most show S_v close to zero in the viscous layer. The reason for the differences from MKM99 are not clear, but it may be worth noting that the spatial resolution of the present hot-film probes is apparently better in the streamwise and spanwise directions than the DNS which uses a grid with $\Delta x^+ \approx 18$ and $\Delta z^+ \approx 6$. The differences with increasing pressure gradients are less than the estimated experimental uncertainties so one cannot claim that the apparent trends are valid. However, one may discern that the run with maximum acceleration shows lower values than the fully developed runs for $y^+ < 8$ and higher ones for $y^+ > 10$; one then sees that such observations are consistent with the comments above concerning the effects of the pressure gradient on the peaks of $N'\{v^+\}$ in the examination of the probability density distributions.

For F_v, as with the measurements of others, the present data converge with the DNS predictions towards the outer edge of the viscous layer (figure 9*b*). In 1994, Thiele & Eckelmann commented that an experimental verification of the values calculated by KMM for $y^+ < 20$ had not been possible to that date; for $y^+ > \sim 15$, the present fully developed measurements agree closely with the database of MKM99 at their lowest Reynolds number (essentially equivalent to KMM and MKM88). However, with the exception of a few points by Thiele & Eckelmann (1994) at $y^+ < 5$, most data disagree with the large increase predicted by DNS as the wall is approached. Our measurements approximately support the suggestion of Niederschulte *et al.* (1990) that F_v is near constant in this region. At low y^+, there is general agreement with the data of Kreplin & Eckelmann and of Niederschulte *et al.* Again, there is no significant effect of the increases in pressure gradient for the present experiment; differences observed between the highest and lowest values of K_p are about the order of the uncertainty estimates (vertical brackets).

Correlations. Since the mean structure showed only a gradual variation with K_p, when it showed any significant effect at all, the rest of the present study concentrates on the two extremes. Results for the highest streamwise pressure gradient, $K_p \approx -0.02$, are compared to those for $K_p \approx -0.008$, the lowest. The latter is the condition near which much of the earlier structure results have been presented: fully developed flow at the maximum flow rate of the oil channel (Wallace *et al.* 1972; Eckelmann 1974; Randolph 1987). The location of $y^+ \approx 15$ was chosen since it corresponds to the most energetic (and most popular) location for conditional analyses (Blackwelder & Kaplan 1976).

The cross-correlation coefficients are defined as

$$R_{u_i u_j}\{y^+, \tau\} = (1/T) \int_0^T [(u_i\{y^+, t\} u_j\{y^+, t-\tau\})/(u_{i,rms} u_{j,rms})] \, \mathrm{d}t,$$

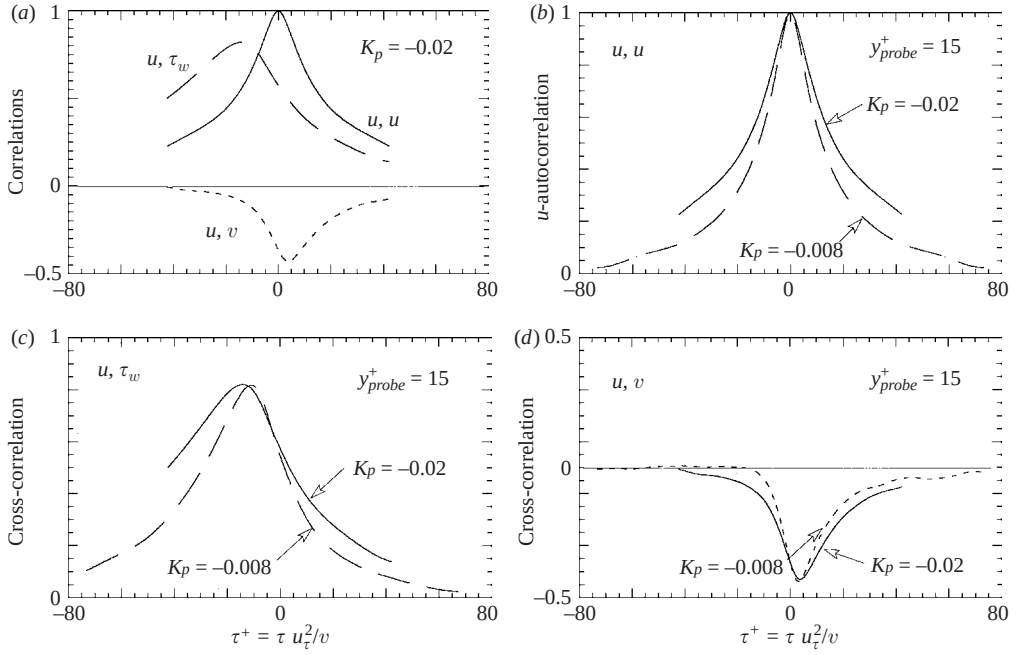

FIGURE 10. Correlation coefficients with cross-wire probe located in the viscous layer ($y^+ \approx 15$): (*a*) laterally converging flow, $K_p \approx -0.020$, (*b*) comparisons of auto-correlations of streamwise velocities (dashed: 'fully developed', $K_p \approx -0.0083$; solid: laterally converging, $K_p \approx -0.020$), (*c*) comparisons of u, τ_w correlations and (*d*) comparisons of u, v correlations (symbols in (*c*) and (*d*) as in (*b*)).

where u_i or u_j represents any of the deduced fluctuation signals and y^+ is the location of the cross-wire probe when involved. Typically, u_i was taken as the streamwise velocity fluctuation, u. With $i = j$, the result reduces to the autocorrelation for the quantity. The results are plotted and presented as correlation coefficients versus non-dimensional lead time τ^+, defined as tu_τ^2/ν where t is the time; to avoid confusion, this symbol is not used to represent normalized shear stress in the present section. (In this section and the next, the symbol τ_w will denote the fluctuation of the wall shear stress rather than its mean.)

Several correlation coefficients for the laterally converging flow at $K_p \approx -0.02$ are compared in figure 10(*a*). For the fully developed flow at $K_p \approx -0.008$, the trends and magnitudes are qualitatively the same. The autocorrelation of the streamwise component peaks at about 1 as it should and shows the expected symmetry. The normal component v shows less correlation with u, both in peak value and duration of significant correlation. The u, v correlation is negative, indicating that v tends to be negative when u is positive and vice versa – a sweep towards the wall corresponds to an increase in u and an ejection to a retardation of u. The greatest u, v correlation is slightly after the peak in the u-autocorrelation, say at $\tau^+ \approx 3$ or so.

The best correlation of τ_w with u is greater than 0.8 and occurs at $\tau^+ \approx -12$. The u, τ_w correlation actually shows a greater correlation between u at $y^+ \approx 15$ and τ_w (i.e. at the wall) than does the correlation between u and v both at $y^+ = 15$, the same location. The peak magnitude is almost twice as large, and the duration is considerably longer. These observations and those of Eckelmann (1974) help to explain the success CMM had in using the temporal wall shear stress for detection in

a VITA sampling technique to deduce average bursting periods of laterally converging flows; while the VITA technique has usually been applied near $y^+ \approx 15$ to detect bursting, the close correlation between τ_w and u permits use of τ_w as an alternative approach.

In figures 10*b*–10*d*, the individual correlations will now be compared directly for the two flow conditions; here the solid curves represent the flow with the larger pressure gradient ($K_p \approx -0.02$) and the dashed lines give the fully developed results for reference.

For the u-autocorrelations (figure 10*b*), by definition both peak at unity at zero lead time, $\tau^+ = 0$. The autocorrelation at $K_p \approx -0.02$ is broader, i.e. greater correlation over a longer non-dimensional time. This result corresponds to the observation of CMM that, as the magnitude of K_p increases, the bursting frequency decreases or the bursting period increases in terms of wall coordinates. The longer average time between randomly occurring bursts would allow eddies to remain coherent longer in the vicinity of the measuring instrument. For the fully developed flow, there seems to be a slight change in the trend of the slope in the range $50 < \tau^+ < 70$, indicating a slightly increased correlation with some phenomenon at τ^+ near 60.

In figure 10(*c*), the peak value of the correlation between u and τ_w is approximately the same for both flows, but it is slightly later (more negative lead time) in the accelerated case. This observation may be a first indication that the inclination of the fronts of the sweep events (Kreplin & Eckelmann 1979*c*) changes with variation of the pressure gradient. As with the other correlations discussed, in the accelerated flow the u, τ_w correlation is broader.

For the u, v correlations (figure 10*d*) – the peak value is almost the same for both as is its lead time; there are minuscule differences, but they are likely less than the typical experimental uncertainty. Again the correlation is broader with the larger pressure gradient. The fully developed results are nearly uncorrelated for $\tau^+ < -15$, whereas the values for $K_p \approx -0.02$ are just approaching zero at the limit of the calculation at $\tau^+ \approx -45$. After the peak, u and v remain slightly more correlated for $K_p \approx -0.02$ than for the fully developed run.

The values of R_{uv} at $\tau^+ = 0$ reveal consistencies in the data and implications for v' (and $\overline{uv}$) that are not obvious from direct examination of v'/u_τ alone. The quantity $R_{uv}\{y^+, \tau^+ = 0\}$ is sometimes called the correlation coefficient (it may be calculated directly from the mean statistics as $\overline{uv}/(u'v')$ without forming the more complete correlation). From this figure, we see it is almost exactly the same for the two extreme cases plotted; the difference is less than 1 %. The Reynolds shear stress $\overline{uv}$ decreases about 50 % from the fully developed flow to the accelerated flow at $y^+ \approx 15$. This decrease is shared somewhat equally between the r.m.s. values, u' and v', in yielding the same value of R_{uv}. However, treating these results in wall coordinates gives a different picture. The quantity $\overline{uv}/u_\tau^2$ decreases (as expected since the total τ/τ_w decreases at this location), but only about 14 %. The corresponding change in non-dimensional r.m.s. values is almost all in the normal component; v'/u_τ decreases about 14 % and u'/u_τ decreases less than 1 %. In other words, if $u'\{y^+\}/u_\tau$ does not show a significant effect due to varying K_p, then $v'\{y^+\}/u_\tau$ must do so – as seen earlier in figure 4(*b*) – in order to remain consistent with the effect on $\tau\{y^+\}/\tau_w$.

The general effects of increasing K_p appear to be a broadening of the correlations over longer non-dimensional times. This observation seems reasonably consistent with the idea that increase of the bursting period (as K_p increases) leads to a better organized flow in the wall region. Longer non-dimensional time scales can be expected

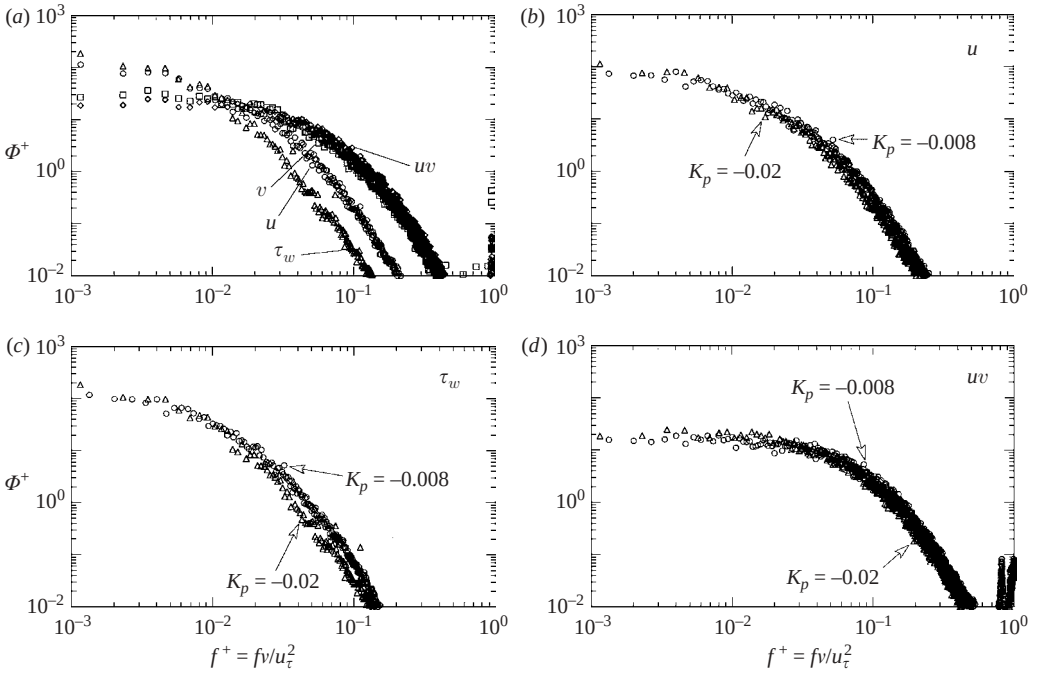

FIGURE 11. Non-dimensional power spectral densities, cross-wire probe located in the viscous layer ($y^+ \approx 15$): (*a*) laterally converging flow, $K_p \approx -0.020$ (circles, u; squares v; upright triangles, τ_w; diamonds, uv), (*b*) streamwise fluctuation (circles, 'fully developed', $K_p \approx -0.0083$; triangles, laterally converging flow, $K_p \approx -0.020$), (*c*) wall shear stress fluctuation and (*d*) fluctuation of the product of u and v fluctuations (symbols in (*c*) and (*d*) as in (*b*)).

to relate to larger non-dimensional length scales, such as the increase in 'linear' layer thickness or the van Driest 'constant' A^+ required in mixing length predictions of the mean velocity profile. That is, the average structures must become larger in terms of non-dimensional wall variables.

Spectra. The power spectral densities for the wall shear stress fluctuations and the velocity fluctuations at $y^+ \approx 15$ are presented in figure 11. These spectra are defined (Brigham 1974; Press *et al.* 1988) as

$$\overline{h^2} = (1/T)\int_0^T |h\{t\}|^2 \,\mathrm{d}t = \int_0^\infty P_h'\{f\}\,\mathrm{d}f = \overline{h^2}\int_0^\infty \Phi_h\{f\}\,\mathrm{d}f,$$

where $h\{t\}$ represents the fluctuation of interest and $P_h'\{f\}$ is its one-sided power spectral density per unit time. They are normalized by division so that

$$\int_0^\infty \Phi_h\{f\}\,\mathrm{d}f = 1.$$

The non-dimensional frequency f^+ and power spectral density Φ_h^+ are based on wall variables (inner scaling). For the spectra of the fluctuations, Φ_u^+, Φ_v^+ or Φ_τ^+, the instantaneous values of the fluctuations are inserted for $h\{t\}$, e.g. $h\{t\} = u\{t\}$ and so forth. For Φ_{uv}^+, we calculate $h\{t\} = (u\{t\}v\{t\} - \overline{uv})$ so it can be considered to be the fluctuation of the product uv (fluctuations themselves) about its mean, the Reynolds shear stress. Thus, Φ_{uv}^+ is not formed from the product of the Fourier transforms of

u and v, which could be considered to give an 'instantaneous Reynolds shear stress' spectrum (or co-spectrum).

For the laterally converging flow at $K_p \approx -0.02$, figure 11(a) shows the comparison of the spectra of the various fluctuating quantities. The least high-frequency content is seen for τ_w; this variable is modulated to some extent by the dominance of molecular transport near the wall and, possibly, by wall conduction effects noted by Alfredsson *et al.* (1988) for the same channel. The spectrum Φ_{uv}^+ has the most high-frequency content, with the v spectrum having almost the same magnitude and with the spectrum for streamwise fluctuations u falling at intermediate values between those of τ_w and of v. This observation indicates that the high-frequency fluctuations for uv are predominantly due to normal fluctuations rather than streamwise ones.

The spectra for the fully developed flow at $K_p \approx -0.008$ show the same trends and approximate magnitudes as the converging flow shown in figure 11(a). That is, the large favourable streamwise pressure gradient does not appear to cause large effects on the non-dimensional spectra at this location.

The other subfigures in figure 11 compare the individual spectra directly for the two extreme cases. In all comparisons, the high-frequency regions of the spectra for the accelerated flow are at lower non-dimensional frequencies than for the fully developed flow. This result is consistent with the apparent broadening of the correlations relative to non-dimensional time. Examining these subfigures, we see Φ_{uv}^+ to be least affected by the strong favourable pressure gradient (figure 11d); results for Φ_v^+ (not shown) are of approximately the same magnitude. While v'/u_τ is apparently lowered about 25 % at $y^+ \approx 15$ for the converging flow compared to the fully developed case, there is no large effect on Φ_u^+ or Φ_{uv}^+ (figures 11b and 11d). The spectra of the wall shear stress fluctuations Φ_τ^+ demonstrate the greatest effect from the strong pressure gradient (figure 11c), but in non-dimensional terms this effect is still not large.

4. Concluding remarks

New fundamental measurements have been obtained for turbulent flow in a converging duct, concentrating on the viscous layer where significant resistances to wall heat, momentum and mass transfer arise. A convergence induces a streamwise acceleration and, thereby, a favourable streamwise pressure gradient.

Provided $-K_p$ is sufficiently small, the viscous layer can be considered to be a constant stress region. In that case, we would expect viscous layer behaviour to be quantitatively the same for boundary layers with or without pressure gradients, converging ducts and fully developed duct flows. A criterion for the reduction in shear stress to be 5 % or less at $y^+ \approx 30$ leads to a threshold value of $-K_p \approx 0.002$ for fully developed turbulent flows; the streamwise momentum equation (Finnicum & Hanratty 1988) indicates that the convective terms moderate the effect of the pressure gradient so the threshold will be slightly higher for accelerating flows. As shown by Patel (1965), $-K_p$ varies inversely with Reynolds number in constant area ducts, so low-Reynolds-number turbulent flows inherently have significant streamwise pressure gradients. Consequently, the first direct numerical simulations for duct flows did not have negligible pressure gradients. For higher values of $-K_p$, wall functions in turbulence models can be expected to become inadequate unless they account for the pressure gradient. A further constraint on generality of viscous layer behaviour is that the boundary condition away from the surface of interest should be located sufficiently far away that there is no significant interaction between that boundary and the viscous layer of concern. An approximate criterion that the distance be

greater than ten times the viscous layer thickness leads to a requirement of 300 wall units or more; for a channel with fully developed flow, this constraint translates to $-K_p \approx 0.003$ or less. Whereas some effects from various geometries can be expected to be qualitatively the same, their magnitudes can be expected to differ at the same value of $-K_p$ when these thresholds are exceeded.

As noted earlier, effects of a favourable streamwise pressure gradient are to reduce bursting rates and to 'thicken' the viscous layer. Consequently, the apparent logarithmic region of the mean streamwise velocity profile is shifted upward as the Reynolds number is lowered or the pressure gradient is increased. At low acceleration parameters, K_v or low $-K_p$, simple turbulence models – such as that of van Driest (1956) – provide adequate predictions of this profile.

The present study extends the earlier work of Eckelmann and colleagues with the same facility and supplements other recent measurements for turbulent flows accelerating in the streamwise direction. The objectives are to determine which features of the turbulence structure remain relatively invariant in the viscous layer, to quantify the variation of the others with moderate to strong streamwise pressure gradients and to confirm or refute the DNS predictions of reductions in $(v')^+$ with increasingly favourable pressure gradients. Use of the oil channel permitted meaningful measurement of the wall-normal component and related statistics in the viscous layer where others could not obtain data owing to problems of spatial resolution. Simultaneous time series data were obtained with an cross-wire probe and a wall sensor to determine $\tilde{u}\{t\}$, $\tilde{v}\{t\}$ and $\tilde{\tau}_w\{t\}$. Measurements with the cross-wire probe at $y^+ \approx 5$, 7, 10, 15, 25 and the centreplane concentrated on four sets of conditions of increasing severity of non-dimensional pressure gradient $-K_p$: two for converging flows and two for fully developed ones. The two sets of data obtained for fully developed flow agreed well with predictions by direct numerical simulations and with measurements by other investigators at low values of the pressure gradient parameter.

Other than the increase of the mean velocity profile, the statistics for the streamwise component suffered no significant effect of pressure gradient. Non-dimensional temporal cross-correlations at $y^+ \approx 15$ broadened slightly. For both high and low $-K_p$, the correlation between u at $y^+ \approx 15$ and the shear stress at the wall is stronger and of longer duration than between u and v at the same location. This observation and the comparable time series by Eckelmann (1974) help to explain the success of Chambers *et al.* (1983) in using a wall sensor to deduce apparent bursting rates in a small converging duct.

The key new results are the measurements of the fluctuating normal component and related statistics in the viscous layer. For $y^+ > \sim 15$, the root-mean-square fluctuation $(v')^+$ decreases as the pressure gradient is increased. This observation supports the trends of the DNS predictions of Spalart (1986) and Finnicum & Hanratty (1988).

The probability density distributions for the instantaneous normal velocity $N'\{\tilde{v}^+\}$ are affected by the streamwise pressure gradient. Towards the outer edge of the viscous layer, the range of values of $\tilde{v}^+$ is broader for the fully developed case than the accelerated case. Since $N'\{\tilde{u}^+\}$ was not significantly affected, this observation implies that the range of angles of the instantaneous velocity vector (Kreplin & Eckelmann 1979*b*) would be less. Comparable probability density distributions were observed for the instantaneous quantity $(\tilde{u}\tilde{v})^+$. The 'tails' of $N'\{(\tilde{u}\tilde{v})^+\}$ in figure 7 appear generally non-symmetric: the values of $N'\{(\tilde{u}\tilde{v})^+\}$ are greater for a given negative value of $(\tilde{u}\tilde{v})^+$ than for the equivalent positive value. Negative values of $(\tilde{u}\tilde{v})^+$ correspond to momentum transport by sweeps and ejections whereas positive

ones are from wallward and outward interactions. This observation is an indication that large values of $|\tilde{u}\tilde{v}|$ are more likely to come from sweeps and ejections than from interactions. Also near the edge, $N'\{(\tilde{u}\tilde{v})^+\}$ distributions in the fully developed run are wider than in the accelerated run. Consequently, we may conclude that another effect of a strong streamwise pressure gradient is to reduce transport of momentum in the outer part of the viscous layer. In conjunction with the trends of $N'\{\tilde{v}^+\}$, this observation implies lessening of the vigour of the ejections as well.

For the higher-order moments of the normal fluctuations, S_v and F_v, the increased experimental uncertainties preclude identifying definite effects of the pressure gradient. However, near the wall our measurements of S_v and F_v and those of others differ from the trends of the DNS predictions – and the differences are greater than the experimental uncertainties. The reason is not clear, but it may be observed that the spatial resolution of the measurements is typically better in the streamwise and spanwise directions than the sizes of the DNS grids.

The study reported was partly supported through the Long Term Research Initiative and Laboratory Directed Research and Development Programs at INL under DoE Idaho Operations Office Contracts DE-AC07-76ID01570, DE-AC07-99ID13727 and DE-AC07-05ID14517. Earlier incarnations were financed by the Applied Hydrodynamics Research Program of the Office of Naval Research (Mr James A. Fein, Program Manager), the National Science Foundation (Dr Win Aung, Program Manager), the US–Deutschland Fulbright Commission, the Max Planck Gesellschaft, the University of Arizona and Westinghouse Naval Systems Division (earlier Gould Ocean Systems Division). To all we are extremely grateful.

The data reduction has principally been via extension of computer programs developed and kindly provided by Michael Randolph. At the former Max Planck Institut für Strömungsforschung, friendly assistance was given by Eduard Bawirzanski, Holger Eisenlohr, Paul Habermann, Ullrich Isermann, Hans-Werner Kompart, Thomas Kowalski, Frank Ohle and Burkhard Thiele, and by Karl-Heinz Nörtemann and Hansjürgen Schäfer with the experiment construction, modifications and preparations. Drs Jovan Jovanovic and Nagi N. Mansour and Professors Robert D. Moser and Peter Bradshaw provided electronic tabulations of measurements and direct numerical simulations. Dr Philippe R. Spalart gave us direct large-scale graphs of the mean statistics predicted by his direct simulations. Several reviewers – both informal and formal – suggested improvements which have made this paper better. Likewise we thank them all.

REFERENCES

Abe, H., Kawamura, H. & Matsuo, Y. 2001 Direct numerical simulation of a fully developed turbulent channel flow with respect to Reynolds number dependence. *Trans. ASME* I: *J. Fluids Engng* **123**, 382–393.

Alfredsson, P. H., Johannsson, A. V., Haritonidis, J. H. & Eckelmann, H. 1988 On the fluctuating wall shear stress and the velocity field in the viscous sublayer. *Phys. Fluids* **31**, 1026–1033.

Bankston, C. A. & McEligot, D. M. 1970 Turbulent and laminar heat transfer to gases with varying properties in the entry region of circular ducts. *Intl J. Heat Mass Transfer* **13**, 319–344.

Becker, S., Stoots, C. M., Condie, K. G., Durst, F. & McEligot, D. M. 2002 LDA-measurements of transitional flows induced by a square rib. *Trans. ASME* I: *J. Fluids Engng* **124**, 108–117.

Berman, N. S. 1978 Drag reduction by polymers. *Annu. Rev. Fluid Mech.* **10**, 47–64.

Blackwelder, R. F. & Eckelmann, H. 1978 The spanwise structure of the bursting phenomenon. *Lecture Notes in Physics* vol. 75, pp. 190–204. Springer.

Blackwelder, R. F. & Kaplan, R. E. 1976 On the wall structure of the turbulent boundary layer. *J. Fluid Mech.* **76**, 86–112.

Blackwelder, R. F. & Kovasznay, L. S. G. 1972 Large scale motion of a turbulent boundary layer during laminarization. *J. Fluid Mech.* **53**, 61–83.

Bradshaw, P. 1975 *An Introduction to Turbulence and its Measurement*, 2nd edn. Pergamon.

Bradshaw, P., Dean, R. B. & McEligot, D. M. 1973 Calculations of interacting turbulent shear layers: Duct flow. *Trans. ASME* I: *J. Fluid Engng* **95**, 214–220.

Brigham, E. O. 1974 *The Fast Fourier Transform* Prentice-Hall.

Brodkey, R. S., Wallace, J. M. & Eckelmann, H. 1974 Some properties of truncated turbulence signals in bounded shear flows. *J. Fluid Mech.* **63**, 209–224.

Castillo, L. & George, W. K. 2001 Similarity analysis for turbulent boundary layer with pressure gradient: outer flow. *AIAA J.* **39**, 41–47.

Chambers, F. W., Murphy, H. D. & McEligot, D. M. 1983 Laterally converging flow. Part 2. Temporal wall shear stress. *J. Fluid Mech.* **127**, 403–428.

Ching, C. Y., Djenidi, L. & Antonia, R. A. 1995 Low-Reynolds-number effects in a turbulent boundary layer. *Exps. Fluids* **19**, 61–68.

van Driest, E. R. 1956 On turbulent flow near a wall. *J. Aerospace Sci.* **23**, 1007–1011, 1036.

Durst, F., Fischer, M., Jovanovic, J. & Kikura, H. 1998 Methods to set up and investigate low Reynolds number, fully developed turbulent plane channel flows. *Trans. ASME* I: *J. Fluids Engng* **120**, 496–503.

Durst, F., Jovanovic, J. & Sender, J. 1995 LDA measurements in the near-wall region of a turbulent pipe flow. *J. Fluid Mech.* **295**, 305–335.

Durst, F., Kikura, H., Lekakis, I., Jovanovic, J. & Ye, Q. 1996 Wall shear stress determination from near-wall mean velocity data in turbulent pipe and channel flows. *Exps. Fluids* **20**, 417–428.

Eckelmann, H. 1974 The structure of the viscous sublayer and the adjacent wall region in a turbulent channel flow. *J. Fluid Mech.* **65**, 439–459.

Eckelmann, H., Nychas, S. G., Brodkey, R. S. & Wallace, J. M. 1977 Velocity and turbulence production in pattern recognized turbulent flow structures. *Phys. Fluids Suppl.* **20**, S225–S231.

Escudier, M. P., Abdel-Hameed, A., Johnson, M. W. & Sutcliffe, C. J. 1998 Laminarisation and re-transition of a turbulent boundary layer subjected to favourable pressure gradient. *Exps. Fluids* **25**, 491–502.

Fernholz, H. H. & Finley, P. 1996 The incompressible zero-pressure-gradient turbulent boundary layer. An assessment of the data. *Prog. Aerospace Sci.* **32**, 245–311.

Fernholz, H. H. & Warnack, D. 1998 The effects of a favourable pressure gradient and of the Reynolds number on an incompressible axisymmetric turbulent boundary layer. Part 1. The turbulent boundary layer. *J. Fluid Mech.* **359**, 329–356.

Finnicum, D. S. & Hanratty, T. J. 1988 Effect of favourable pressure gradients on turbulent boundary layers. *AIChE J.* **34**, 529–540.

Fontaine, A. A. & Deutsch, S. 1995 Three-component, time-resolved velocity statistics in the wall region of a turbulent pipe flow. *Exps. Fluids* **18**, 168–173.

Hanjalic, K., Hadzic, I. & Jakirlic, S. 1999 Modeling turbulent wall flows subjected to strong pressure variations. *Trans. ASME* I: *J. Fluids Engng* **121**, 57–64.

Hanjalic, K., Jakirlic, S. & Hadzic, I. 1997 Expanding the limits of 'equilibrium' second-moment turbulence closures. *Fluid Dyn. Res.* **20**, 25–71.

Harder, K. G. & Tiederman, W. G. 1989 Influence of wall strain rate, polymer concentration and channel height upon drag reduction and turbulent structure. *Tech. Rep.* PME-FM-89-1, Purdue University.

Huffman, G. D. & Bradshaw, P. 1972 A note on von Kármán's constant in low Reynolds number turbulent flows. *J. Fluid Mech.* **53**, 45–60.

Ichimiya, M. 1995 Properties in a relaminarizing turbulent boundary layer under a favourable pressure gradient. *Proc. 10th Symp. Turb. Shear Flow, University Park, Penna*, pp. 11-7–11-12.

Johnson, F. D. & Eckelmann, H. 1983 Has a small-scale structure in turbulence been experimentally verified? *Phys. Fluids* **26**, 2406–2414.

Jones, M. B., Marusic, I. & Perry, A. E. 2001 Evolution and structure of sink-flow boundary layers. *J. Fluid Mech.* **428**, 1–27.

Jones, W. C. & Launder, B. E. 1972 Some properties of sink–flow turbulent boundary layers. *J. Fluid Mech.* **56**, 337–351.

Julien, H. L., Kays, W. M. & Moffat, R. J. 1969 The turbulent boundary layer on a porous plate: Experimental study of the effects of a favourable pressure gradient. *Tech. Rep.* HMT-4, Thermosci. Div., Mech. Engr. Dept, Stanford University.

Kays, W. M. & Crawford, M. E. 1980 *Convective Heat and Mass Transfer*, 2nd edn. McGraw-Hill.

Kim, J., Moin, P. & Moser, R. D. 1987 Turbulent statistics in fully developed channel flow at low Reynolds number. *J. Fluid Mech.* **177**, 133–166.

Klewicki, J. C. & Falco, R. E. 1990 On accurately measuring statistics associated with small-scale structure in turbulent boundary layers using hot-wire probes. *J. Fluid Mech.* **219**, 119–142.

Kline, S. J., Reynolds, W. C., Schraub, F. A. & Rundstadler, P. W. 1967 The structure of turbulent boundary layers. *J. Fluid Mech.* **30**, 741–773.

Kreplin, H.-P. 1973 Eine Methode zur Linearisierung von Heissfilmsignalen mit dem Digitalrechner PDP-15 und ihre Anwendung bei Messungen in einer turbulenten Kanalströmung. Rep. 2/1973, Max Planck Institut für Strömungsforschung, Göttingen. Diplomarbeit, University of Göttingen.

Kreplin, H.-P. 1976 Experimentelle Untersuchung der Längsschwankungen und der wandparallelen Querschwankungen der Geschwindigkeit in einer turbulenten Kanalströmung. Mitt. no. 63/1976, Max Planck Institut für Strömungsforschung und AVA Göttingen. PhD dissertation, University of Göttingen.

Kreplin, H.-P. & Eckelmann, H. 1979*a* Propagation of perturbations in the viscous sublayer and adjacent wall region. *J. Fluid Mech.* **95**, 305–322.

Kreplin, H.-P. & Eckelmann, H. 1979*b* Instantaneous direction of the velocity vector in a fully-developed turbulent channel flow. *Phys. Fluids* **22**, 1210–1211.

Kreplin, H.-P. & Eckelmann, H. 1979*c* Behaviour of the three fluctuating velocity components in the wall region of a turbulent channel flow. *Phys. Fluids* **22**, 1233–1239.

Launder, B. E. 1964 Laminarization of the turbulent boundary layer by acceleration. MIT Gas Turbine Lab. Rep. 77. Also NASA N66-16042.

Launder, B. E. & Jones, W. P. 1969 Sink flow turbulent boundary layers. *J. Fluid Mech.* **38**, 817–831.

Loyd, R. J., Moffat, R. J. & Kays, W. M. 1970 The turbulent boundary layer on a porous plate: an experimental study of the fluid dynamics with strong favourable pressure gradient and blowing. *Tech. Rep.* HMT-13, Thermosci. Div., Mech. Engr. Dept, Stanford University.

McEligot, D. M. 1984 Measurement of wall shear stress in accelerating turbulent flows. Bericht 109/1984, Max Planck Inst. für Strömungsf., Göttingen, BRD.

McEligot, D. M. 1985 Measurement of wall shear stress in favourable pressure gradients. *Lecture Notes in Physics* **235**, 292–303.

McEligot, D. M. & Bankston, C. A. 1969 Numerical predictions for circular tube laminarization by heating. *ASME Paper* 69-HT-52, National Heat Transfer Conference, Minneapolis.

McEligot, D. M. & Eckelmann, H. 2003 Effects of laterally converging flows on mean turbulence structure in the viscous layer. Tech. Rep. INEEL/EXT-2002-697, Idaho National Engineering and Environmental Laboratory.

McEligot, D. M., Ormand, L. W. & Perkins, H. C. 1966 Internal low Reynolds number turbulent and transitional gas flow with heat transfer. *Trans. ASME* C: *J. Heat Transfer* **88**, 239–245.

Mansour, N. N., Kim, J. & Moin, P. 1988. Reynolds-stress and dissipation-rate budgets in a turbulent channel flow. *J. Fluid Mech.* **194**, 15–44.

Marks, L. S. (ed.) 1916 *Mechanical Engineers' Handbook*. McGraw-Hill.

Mayle, R. E. 1991 The role of laminar–turbulent transition in gas turbine engines. *J. Turbomachinery* **113**, 509–537.

Metzger, M. M. 2002 Scalar dispersion in high Reynolds number turbulent boundary layers. PhD thesis, University of Utah.

Metzger, M. M. & Klewicki, J. C. 2001 A comparative study of near-wall turbulence in high and low Reynolds number boundary layers. *Phys. Fluids* **13**, 692–701.

Moin, P. & Spalart, P. R. 1988 Contributions of numerical simulation data bases to the physics, modeling, and measurement of turbulence. *Advances in Turbulence* (ed. W. K. George & R. Arndt), pp. 11–38. Hemisphere.

Morrow, T. B. & Kline, S. J. 1971 The evaluation and use of hot-wire and hot-film anemometers in liquids. Rep. MD-25, Mech. Engr. Dept., Stanford University.

Moser, R. D., Kim, J. & Mansour, N. N. 1999 Direct numerical simulation of turbulent channel flow up to $Re_\tau = 590$. *Phys. Fluids* **11**, 943–945.

Murphy, H. D. 1979 Flow near the outlet of a geothermal energy reservoir. PhD thesis, University of Arizona. Also Rep. LA-7906-T, available from the National Technical Information Service.

Murphy, H. D., Chambers, F. W. & McEligot, D. M. 1983 Laterally converging flow. Part 1. Mean flow. *J. Fluid Mech.* **127**, 379–401.

Murphy, H. D., Coxon, M. & McEligot, D. M. 1978 Symmetric sink flow between parallel plates. *Trans. ASME* I: *J. Fluids Engng* **100**, 477–484.

Narasimha, R. & Sreenivasan, K. R. 1979 Relaminarization of fluid flows. *Adv. Appl. Mech.* **19**, 221–309.

Niederschulte, M. A., Adrian, R. J. & Hanratty, T. J. 1990 Measurements of turbulent flow in a channel at low Reynolds numbers. *Exps. Fluids* **9**, 222–230.

Nikolaides, C. 1984 A study of coherent structures in the viscous wall region of a turbulent flow. PhD thesis, University of Illinois.

Panton, R. L. & Linebarger, J. H. 1974 Wall pressure spectrum calculations for equilibrium boundary layers. *J. Fluid Mech.* **65**, 261–287.

Patel, V. C. 1965 Calibration of the Preston tube and limitations on its use in pressure gradients. *J. Fluid Mech.* **23**, 185–208.

Press, W. H., Flannery, B. P., Tenkolsky, S. A. & Vetterling, W. T. 1988 *Numerical Recipes in C; the Art of Scientific Computing*. Cambridge University Press.

Randolph, M. 1983 Experimentelle Untersuchung der Längsschwankungen und der wandnormalen Querschwankungen der Geschwindigkeit in einer turbulenten Kanalströmung. Diplomarbeit, University of Göttingen.

Randolph, M. 1987 Experimentelle Untersuchung in einer turbulenten Kanalströmung zur Erkennung von Fronten hoher Geschwindigkeit und Klärung ihres Zusammengangs mit Streifen kleiner Geschwindigkeit und Längswirbeln. PhD thesis, University of Göttingen.

Reichardt, H. 1938 Messungen turbulenter Schwankungen. *Naturwissenschaften* **26**, 404–408.

Reynolds, H. C. 1969 Internal low Reynolds number turbulent heat transfer. PhD thesis, University of Arizona.

Rodi, W. 1980 *Turbulence Models and their Application in Hydraulics*. IAHR, Delft.

Sano, M. & Asako, Y. 1993 Fluid flow and heat transfer in a periodically diverging–converging turbulent duct flow. *JSME Intl J.* B **36**, 207–213.

Sano, M. & Shirakashi, M. 1994 Statistical characteristics of turbulence in a periodically diverging–converging channel flow. *JSME Intl J.* B **37**, 782–788.

Schlichting, H. 1968 *Boundary Layer Theory*, 6th edn. McGraw-Hill.

Senecal, V. E. 1952 Fluid flow in the transition zone. PhD thesis, Carnegie Inst. Tech.

Shehata, A. M. & McEligot, D. M. 1998 Mean turbulence structure in the viscous layer of strongly-heated internal gas flows. Measurements. *Intl J. Heat Mass Transfer* **41**, 4297–4313.

Singh, A., Vyas, B. D. & Powle, U. S. 1999 Investigations on inward flow between two stationary parallel disks. *Intl J. Heat Fluid Flow* **20**, 395–401.

Spalart, P. R. 1986 Numerical study of sink–flow boundary layers. *J. Fluid Mech.* **172**, 307–328.

Spalart, P. R. & Watmuff, J. H. 1993 Experimental and numerical study of a turbulent boundary layer with pressure gradients. *J. Fluid Mech.* **249**, 337–371.

Suzuki, Y. & Kasagi, N. 1992 Evaluation of hot-wire measurements in wall shear turbulence using a direct numerical simulation database. *Exps. Thermal Fluid Sci.* **5**, 69–77.

Thiele, B. & Eckelmann, H. 1994 Application of a partly submerged two component laser-Doppler anemometer in a turbulent flow. *Exps. Fluids* **17**, 390–396.

Wallace, J. M., Brodkey, R. S. & Eckelmann, H. 1977 Pattern-recognized structures in bounded turbulent shear flows. *J. Fluid Mech.* **83**, 673–693.

Wallace, J. M., Eckelmann, H. & Brodkey, R. S. 1972 The wall region in turbulent shear flows. *J. Fluid Mech.* **54**, 39–48.

Warnack, D. & Fernholz, H. H. 1998 The effects of a favourable pressure gradient and of the Reynolds number on an incompressible axisymmetric turbulent boundary layer. Part 2. The boundary layer with relaminarization. *J. Fluid Mech.* **359**, 357–381.

Willmarth, W. W. & Lu, S. S. 1972 Structure of the Reynolds stress near the wall. *J. Fluid Mech.* **55**, 65–92.